

# *Validation of OMI erythemal doses with multi-sensor ground-based measurements in Thessaloniki, Greece*

Article

Accepted Version

Creative Commons: Attribution-Noncommercial-No Derivative Works 4.0

Zempila, M. M., Fountoulakis, I., Taylor, M., Kazadzis, S., Arola, A., Koukouli, M. E., Bais, A., Meleti, C. and Balis, D. (2018) Validation of OMI erythemal doses with multi-sensor ground-based measurements in Thessaloniki, Greece. *Atmospheric Environment*, 183. pp. 106-121. ISSN 13522310 doi: <https://doi.org/10.1016/j.atmosenv.2018.04.012> Available at <http://centaur.reading.ac.uk/77161/>

It is advisable to refer to the publisher's version if you intend to cite from the work. See [Guidance on citing](#).

Published version at: <http://dx.doi.org/10.1016/j.atmosenv.2018.04.012>

To link to this article DOI: <http://dx.doi.org/10.1016/j.atmosenv.2018.04.012>

Publisher: Elsevier

All outputs in CentAUR are protected by Intellectual Property Rights law, including copyright law. Copyright and IPR is retained by the creators or other copyright holders. Terms and conditions for use of this material are defined in the [End User Agreement](#).

[www.reading.ac.uk/centaur](http://www.reading.ac.uk/centaur)

## **CentAUR**

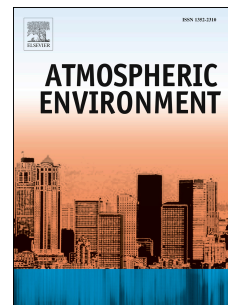
Central Archive at the University of Reading

Reading's research outputs online

# Accepted Manuscript

Validation of OMI erythemal doses with multi-sensor ground-based measurements in Thessaloniki, Greece

Melina Maria Zempila, Ilias Fountoulakis, Michael Taylor, Stelios Kazadzis, Antti Arola, Maria Elissavet Koukouli, Alkiviadis Bais, Chariklia Meleti, Dimitrios Balis



PII: S1352-2310(18)30237-1

DOI: [10.1016/j.atmosenv.2018.04.012](https://doi.org/10.1016/j.atmosenv.2018.04.012)

Reference: AEA 15945

To appear in: *Atmospheric Environment*

Received Date: 12 December 2017

Revised Date: 3 April 2018

Accepted Date: 8 April 2018

Please cite this article as: Zempila, M.M., Fountoulakis, I., Taylor, M., Kazadzis, S., Arola, A., Koukouli, M.E., Bais, A., Meleti, C., Balis, D., Validation of OMI erythemal doses with multi-sensor ground-based measurements in Thessaloniki, Greece, *Atmospheric Environment* (2018), doi: 10.1016/j.atmosenv.2018.04.012.

This is a PDF file of an unedited manuscript that has been accepted for publication. As a service to our customers we are providing this early version of the manuscript. The manuscript will undergo copyediting, typesetting, and review of the resulting proof before it is published in its final form. Please note that during the production process errors may be discovered which could affect the content, and all legal disclaimers that apply to the journal pertain.

1 **VALIDATION OF OMI ERYTHEMAL DOSES WITH MULTI-SENSOR GROUND-**  
2 **BASED MEASUREMENTS IN THESSALONIKI, GREECE**

3  
4 **Melina Maria Zempila**<sup>(1\*,2)</sup>, **Ilias Fountoulakis**<sup>(2)</sup>, **Michael Taylor**<sup>(3)</sup>, **Stelios Kazadzis**<sup>(4,5)</sup>, **Antti**  
5 **Arola**<sup>(6)</sup>, **Maria Elissavet Koukoulis**<sup>(2)</sup>, **Alkiviadis Bais**<sup>(2)</sup>, **Chariklia Meleti**<sup>(2)</sup>, **Dimitrios Balis**<sup>(2)</sup>

6 <sup>(1)</sup> Laboratory of Atmospheric Physics, Aristotle University of Thessaloniki, PO Box 149, 54124,  
7 Thessaloniki, Greece.

8 <sup>(2)</sup> RAL Space, UK Research and Innovation, Rutherford Appleton Laboratory, Harwell Oxford,  
9 Didcot OX11 0QX, United Kingdom.

10 <sup>(3)</sup> Department of Meteorology, University of Reading, Reading, RG6 6BB, United Kingdom.

11 <sup>(4)</sup> Physikalisch-Meteorologisches Observatorium Davos, World Radiation Center, Dorfstrasse 33,  
12 7260 Davos Dorf, Switzerland.

13 <sup>(5)</sup> Institute of Environmental Research and Sustainable Development, National Observatory of  
14 Athens, Greece.

15 <sup>(6)</sup> Finnish Meteorological Institute, FI-70211 Kuopio, Finland.

16  
17 \*Correspondence author: melina.zempila@stfc.ac.uk

18  
19 **ABSTRACT**

20 The aim of this study is to validate the Ozone Monitoring Instrument (OMI) erythemal dose rates  
21 using ground-based measurements in Thessaloniki, Greece. In the Laboratory of Atmospheric  
22 Physics of the Aristotle University of Thessaloniki, a Yankee Environmental System UVB-1  
23 radiometer measures the erythemal dose rates every minute, and a Norsk Institutt for Luftforskning  
24 (NILU) multi-filter radiometer provides multi-filter based irradiances that were used to derive  
25 erythemal dose rates for the period 2005-2014. Both these datasets were independently validated  
26 against collocated UV irradiance spectra from a Brewer MkIII spectrophotometer. Cloud detection  
27 was performed based on measurements of the global horizontal radiation from a Kipp & Zonen  
28 pyranometer and from NILU measurements in the visible range. The satellite versus ground  
29 observation validation was performed taking into account the effect of temporal averaging,  
30 limitations related to OMI quality control criteria, cloud conditions, the solar zenith angle and  
31 atmospheric aerosol loading. Aerosol optical depth was also retrieved using a collocated CIMEL  
32 sunphotometer in order to assess its impact on the comparisons. The effect of total ozone columns

33 satellite versus ground-based differences on the erythemal dose comparisons was also investigated.  
34 Since most of the public awareness alerts are based on UV Index (UVI) classifications, an analysis  
35 and assessment of OMI capability for retrieving UVIs was also performed.

36 An overestimation of the OMI erythemal product by 3-6% and 4-8% with respect to ground  
37 measurements is observed when examining overpass and noontime estimates respectively. The  
38 comparisons revealed a relatively small solar zenith angle dependence, with the OMI data showing  
39 a slight dependence on aerosol load, especially at high aerosol optical depth values. A mean  
40 underestimation of 2% in OMI total ozone columns under cloud-free conditions was found to lead  
41 to an overestimation in OMI erythemal doses of 1 - 5%. While OMI overestimated the erythemal  
42 dose rates over the range of cloudiness conditions examined, its UVIs were found to be reliable for  
43 the purpose of characterizing the ambient UV radiation impact.

44

#### 45 **KEYWORDS**

46 Erythemal, CIE, UV index, OMI, Validation, NILU-UV, UVB-1, BREWER, CM21, YES, PAR,  
47 CIMEL, Neural Network, Thessaloniki, Greece.

## 48 1. INTRODUCTION

49 Changes in climate and atmospheric composition may lead to unprecedented changes in the  
50 Ultraviolet (UV) radiation that reaches the Earth's surface, raising the concern of indirect and direct  
51 effects to plants, ecosystems and humans (IPCC AR5, 2014; Tevini, 1993; WMO, 2007; WHO,  
52 2008; Gao, Schmoldt, and Slusser, 2010; among others). Since 1982, when the ozone depletion was  
53 firstly observed (e.g. Farman et al., 1985; Bhartia et al., 1985), ground-based UV monitoring sites  
54 have been deployed at several locations all over the globe as a response to the raising concern of  
55 potential enhanced surface UV levels (Ghetti, Checcucci and Bornman, 2006). Most of these sites  
56 nowadays provide high frequency measurements for a variety of surface UV radiation products,  
57 such as the erythemal weighted dose rates, UV index, and so on. These data are used to validate  
58 model projections and satellite estimates, and to alert public awareness regarding the effects of the  
59 exposure to high solar UV radiation levels (Schmalwieser et al., 2002; Gies et al., 2004; Taskanen  
60 et al., 2007; Weihs et al., 2008; McKenzie et al., 2001; WHO, 2008; among others).

61 Up-to-date, space-borne UV product estimates originate from a variety of instruments onboard  
62 different platforms (Arola et al., 2002; Taskanen et al., 2006). One of them is the Ozone Monitoring  
63 Instrument (OMI) on board the Aura platform that provides estimates of surface erythemal dose  
64 rates and daily doses at overpass and noontime along with UV index (UVI) values since its launch  
65 in July 2004. Studies on OMI UV products (irradiances, erythemal doses and UV index) have  
66 reported differences of up to 30% or even higher under certain conditions overestimation in OMI  
67 UV products when compared with corresponding ground-based measurements, while these  
68 discrepancies were mainly observed at urban areas with higher aerosol loads (Kazadzis et al.,  
69 2009a; Kazadzis et al., 2009b; Ialongo et al., 2010; Antón et al. 2010; Cachorro et al., 2010; A Jebar  
70 et al., 2017). In 2009, a study by Arola et al. (2009) introduced a correction on the OMI data for  
71 absorbing aerosols which led to smaller discrepancies between OMI and ground-based data, with  
72 OMI performance being improved due to the imposed aerosol correction (Mateos et al., 2013;  
73 Muyimbwa et al., 2015; Cadet et al., 2017; Bernhard et al., 2015).

74 In this study, OMI UV erythemal dose rates and UVI values at overpass and local noontimes were  
75 thoroughly evaluated in Thessaloniki, Greece (lat: 40.69° N, lon: 22.96° E, alt: 60 m) for the period  
76 2005-2014, using a suite of ground-based instruments located at the Laboratory of Atmospheric  
77 Physics (LAP), at the Aristotle University of Thessaloniki, Greece together with retrieval models.  
78 The influence of solar zenith angle (SZA), total ozone column (TOC) and aerosol optical depth  
79 (AOD) on the satellite UV products was also analysed, while the impact of three basic types of

80 cloudiness conditions defined as: unstable cloudy (partially covered sun disk), stable cloudy (fully  
81 covered sun disk), and unoccluded sun disk, were also investigated.

82 Consequently, this study provides an innovative, complete and in-depth evaluation of the erythemal  
83 products provided by OMI/Aura, where the synergy of a wide suite of ground-based measurements  
84 is proven invaluable in order to examine, quantify and eventually unfold the dynamics of all the  
85 parameters potentially affecting the satellite retrievals.

86 The backbone of the paper is as follows. In Section 2 the ground-based instrumentation with the  
87 corresponding measurements are provided, while the OMI measurements are presented in the  
88 second subsection. In the following section (Section 3), the methodology applied to retrieve  
89 erythemal dose rates from irradiance measurements originating from the NILU-UV multi-filter  
90 radiometer is analysed, and the results are validated against collocated erythemal dose rate  
91 measurements from the UVB-1 radiometer placed also in the site. Then, the evaluation of the OMI  
92 erythemal dose rates is presented in Section 4, where the influence of the SZA, ozone, aerosols and  
93 cloudiness type is examined. At the end of the same section, the UV index comparisons are  
94 presented in order to elaborate on the ability of OMI UV Index estimations to serve as a public alert  
95 source, especially during the summer when the impact of the exposure to excess UV doses is more  
96 detrimental. The study concludes with its 5<sup>th</sup> and final section by summarizing the main findings of  
97 the validation process.

98

## 99 **2. DATASETS AND INSTRUMENTATION**

### 100 **2.1. Ground-based measurements**

101 At the Laboratory of Atmospheric Physics at Aristotle University of Thessaloniki, Greece,  
102 (LAP/AUTH: <http://lap.physics.auth.gr>) three different types of solar radiation sensors provide  
103 estimates of erythemal dose rates continuously since 2005 as per the joint International  
104 Organisation for Standardisation and Commission Internationale de l'Éclairage standard ISO  
105 17166:1999(E)/CIE S 007-1998 (and which we will abbreviate as 'CIE' here). For each instrument,  
106 different methods were applied in order to derive the erythemal dose rates, based on the  
107 characteristics of the measurements and the technical aspects of each instrument.

108 A Brewer MkIII spectrophotometer with serial number #086 (B086) measures the UV solar  
109 spectrum (286.5 - 363 nm) with a wavelength step of 0.5 nm at LAP since 1993. It is equipped with  
110 a double monochromator which is eliminating influences of stray light (scattered photons/signal at  
111 one wavelength that is affected by radiation from other wavelengths) in the measurements, thus

112 providing better accuracy especially in the shorter UV wavelengths (Zerefos and Bais, 1997;  
113 Karppinen et al., 2014). The uncertainty in the B086 spectra that are used in this study is 5% for  
114 wavelengths higher than 305 nm and solar zenith angles (SZA) smaller than  $80^\circ$  (Fountoulakis et  
115 al., 2016a), while low recorded signals at lower wavelengths and higher SZAs lead to higher  
116 uncertainties in the measurements (Fountoulakis et al., 2016b; Gröbner et al., 2006). In order to  
117 obtain solar spectra up to 400 nm, the SHICrvm algorithm (Slaper et al., 1995) has been applied to  
118 the original data, while the outcome was weighted with the erythemal dose action spectrum  
119 (McKinlay & Diffey, 1987) and integrated over the nominal wavelength range. Although B086  
120 provides high accuracy erythemal dose rates, the frequency of the measurements is one every 20-40  
121 minutes while a complete scan lasts  $\sim 7$  minutes. Therefore, even though B086 scans cannot capture  
122 high frequency changes in the radiation field, these measurements provide a unique tool to monitor  
123 and assess the stability of other instruments that provide measurements with higher frequency  
124 (Zempila et al., 2016a).

125 A Yankee Environmental System (YES) UVB-1 radiometer has also been operating since 1991.  
126 The UVB-1 is a broadband instrument with a spectral response that simulates the erythemal action  
127 spectrum proposed by McKinlay & Diffey (1987) and thus provides erythemal dose measurements  
128 on a 1-minute basis. Using libRadtran radiative transfer model simulations (Emde et al., 2015), look  
129 up tables are calculated with respect to SZA and the TOC which are used to convert the UVB-1  
130 measurements into erythemal irradiance due to differences between the actual and the desired  
131 spectral response (Lantz & Disterhoft, 1998; Webb et al., 2006;). The TOC values for these  
132 corrections are obtained from collocated measurements from a second Brewer spectrophotometer  
133 with serial number 005 (B005) (Meleti et al., 2012, Zerefos et al., 2002, Fragkos et al. 2014,  
134 Fragkos et al. 2016). Under clear (cloudless) skies, the erythemal irradiances from B086 and UVB-  
135 1 (within one minute from the mean time of the B086 scan) have shown a satisfactory agreement;  
136 within 4% ( $1\sigma$ ) for SZAs less than  $80^\circ$  for the period 2004 – 2014, that is in compliance with the  
137 results presented in Hülsen et al. (2008). This agreement testifies that UVB-1 erythemal dose rates  
138 have similar uncertainty level with the ones derived from B086 UV spectra (Garane et al., 2006;  
139 Bais et al., 1996; Bais et al., 2001). Periodic intercalibrations of UVB-1 and B086 ensure the long-  
140 term stability of the instrument.

141 A Norsk Institutt for Luftforskning (NILU)-UV multi-filter radiometer has been operational since  
142 2005 and forms part of the Greek UV network of NILU-UV radiometers (Kazantzidis et al., 2006).  
143 The NILU-UV with serial number 04103 provides 1-minute measurements in 5 UV channels with



144 nominal central wavelength at 302, 312, 320, 340 and 380 nm and a full width at half maximum  
145 (FWHM) of 10 nm. The instrument is also equipped with an additional channel that measures the  
146 photosynthetically active radiation (PAR). In this study, measurements of the PAR channel were  
147 used to determine cloud-free cases based on the cloud detection algorithm proposed by Zempila et  
148 al., 2016b. By calibrating the NILU measurements with the B086 coincident irradiances, we  
149 estimate that the uncertainties of the NILU irradiance measurements used in this study are less than  
150 5.5% (Zempila et al., 2016a). In Section 3 a description of the methodology used to derive  
151 erythemal dose rates from the NILU UV irradiances measurements is provided, while comparisons  
152 with UVB-1 measurements are presented in the second part of the section.

153 Additionally at LAP, a CM21 (Kipp&Zonen) pyranometer provides global horizontal irradiance  
154 (GHI) measurements at one-minute intervals along with the corresponding standard deviation.  
155 Although the manufacturer states that the CM type of pyranometers have a stability of less than  
156  $\pm 0.5\%$ /year, recalibration of the instrument that took place in 2005 revealed a high stability in its  
157 sensitivity with changes less than 0.1% during its 12 years of continuous operation (Bais et al.,  
158 2013). According to Zempila et al. (2016c) the maximum uncertainty inherent in the CM21  
159 measurements is 6.4% based on error propagation techniques, while its records can provide  
160 information on the cloudiness status, distinguishing cases where the sun is unoccluded or  
161 fully/partially covered by clouds based on the methodology described by Vasaras et al. (2001). This  
162 information is used to further investigate the cloud effect on the satellite against ground-based  
163 erythemal dose rate comparisons.

164 Furthermore, a CE318-N Sun Sky photometer (CIMEL) provides atmospheric observations as part  
165 of the NASA aerosol robotic network (AERONET) (Holben et al., 1998; Balis et al., 2010). CIMEL  
166 provides AOD at the 340 nm wavelength, which is used to investigate the effect of aerosol  
167 variability over the station within the comparisons between the satellite- and ground-based  
168 erythemal data.

169

## 170 **2.2. Satellite measurements**

171 OMI is a contribution of the Netherlands's Agency for Aerospace Programs (NIVR) in collaboration  
172 with the Finnish Meteorological Institute (FMI) to the Earth Observing System (EOS) Aura  
173 platform. OMI is a nadir viewing hyperspectral imager capable of measuring the backscatter solar  
174 radiation in the UV and visible. With its high spectral resolution (0.45 nm), OMI is able to provide  
175 high accuracy estimations of several atmospheric parameters (Levelt et al., 2006). OMI scans in 740

176 wavelength bands with a swath width of 2600 km that allows OMI to view the globe within one day  
177 (14 orbits). With its optimal  $13 \times 24 \text{ km}^2$  spatial resolution, OMI footprint centered to Thessaloniki  
178 coordinates, is covered by 50% of urban area while the city suburbs, rural area and the sea (with  
179 coverage of 25%) occupy the rest half percentage. The OMI surface UV irradiance data include the  
180 erythemally-weighted daily doses and the dose rates both at the overpass time (mean Thessaloniki  
181 visiting time: 11:45 UT) and at the local solar noon (mean Thessaloniki local noon time: 10:26 UT).  
182 For this study, surface UV overpass data for Thessaloniki have been extracted from the NASA Aura  
183 Data Validation Centre for the period 2005-2014, <http://avdc.gsfc.nasa.gov/>. The OMI retrieval  
184 algorithm estimates the clear-sky surface irradiance using as inputs to radiative transfer model basic  
185 geophysical information, the measured total ozone column and climatological surface albedo  
186 (Torres et al., 2007 and references therein). Then, the clear-sky irradiances are adjusted to real  
187 scene values by a transmittance factor that is derived from the ratio of the backscattered radiance  
188 over the solar irradiances at 360 nm accounting for both clouds and scattering aerosols. Currently  
189 the UV algorithm uses a monthly aerosol climatology to also correct for absorbing aerosols (Arola  
190 et al., 2009). Regarding the cloud information, the radiative transfer model does not account for  
191 broken, multi-layer or mixed phase clouds resulting in more noisy comparisons with ground-based  
192 measurements under cloudy conditions. Furthermore, the derivation of the local noon values does  
193 not take into account changes in cloudiness, ozone and aerosols between local noon and overpass  
194 time, introducing higher uncertainty in the local noon retrievals (Torres et al., 2007). More details  
195 regarding the OMI UVB algorithm can be found in the Algorithm Theoretical Basis Document  
196 (Krotkov et al., 2002) and examples of its validation may be viewed in Tanskanen et al. (2007),  
197 Arola et al. (2009), and, specifically for Thessaloniki, in Kazadzis et al. (2009a; 2009b).

198

### 199 **3. The NILU-UV Erythemal product**

#### 200 **3.1. Effective UV doses from NILU-UV irradiances using a neural network model**

201 To retrieve the effective UV dose rates from the original NILU irradiance measurements, a feed-  
202 forward function-approximating neural network (NN) model (Hornik, Stinchcombe and White,  
203 1989) was coded using MATLAB's object-oriented scripting language in conjunction with its  
204 Neural Network Toolbox (Beale, Hagan and Demuth, 2012). As inputs, the NN has NILU  
205 irradiance measurements at 302, 312, 320, 340 and 380 nm and various temporal variables  
206 (Kolehmainen, Martikainen and Ruuskanen, 2001) including the SZA, the day of the week (DOW)  
207 and the day of the year (DOY) and its sinusoidal components. The target (output) variable is the

208 erythemal UV dose rate resulting from B086 erythemal weighted spectra.  
 209 From the available data, 47908 co-located input-output vectors were extracted to train and validate  
 210 the NN model. As per the NN method described in Zempila et al (2017b), the input and output  
 211 vectors were connected via 2 network layers – the first containing hidden neurons with hyperbolic  
 212 tangent (tanh) activation functions and the second containing linear activation functions. The NN  
 213 architecture was optimized following the method of Taylor et al (2014) where the number of hidden  
 214 neurons was varied from 5 to 15 and the proportion of training data used in NN learning was varied  
 215 from 50% to 95% in steps of 5% with a mean squared error (MSE) cost function measuring the  
 216 difference in NN retrievals and target erythemal dose rates for 100 different NN architectures. The  
 217 optimal NN has a training proportion of 90% and 13 hidden neurons and used the same NN learning  
 218 scheme based on Bayesian regularization back-propagation described in Zempila et al (2017b).  
 219 In **Error! Reference source not found.**the range of the validity of the trained optimal NN is  
 220 provided based on the input data range of the subset used to train the model. The addition temporal  
 221 variables are not listed as they have the standard ranges (see Zempila et al (2017b) for details).

222  
 223 **Table 1.** Range of validity of the trained optimal NN as determined by its input parameters (upper  
 224 list) and output parameters (lower list).

Parameter	Min	Max	Mean	St. Dev.
Ir (305) (W/m <sup>2</sup> /nm)	0	0.017	0.003	0.004
Ir(312) (W/m <sup>2</sup> /nm)	0	0.229	0.064	0.055
Ir(320) (W/m <sup>2</sup> /nm)	0	0.333	0.108	0.079
Ir(340) (W/m <sup>2</sup> /nm)	0	0.678	0.252	0.159
Ir(380) (W/m <sup>2</sup> /nm)	0	0.871	0.327	0.208
SZA (Degrees)	15.63	81.162	54.373	16.120
Erythemal dose rate (W/m <sup>2</sup> )	0	0.234	0.056	0.054

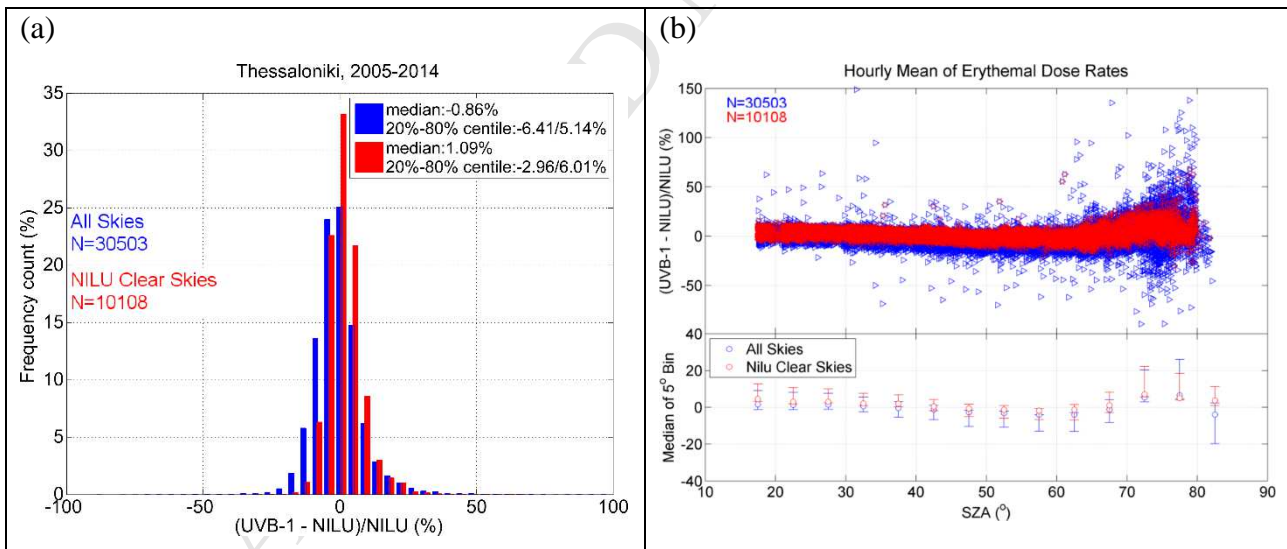
225  
 226 Following the approach of Zempila et al (2017b), the trained and validated NN was then run in  
 227 unsupervised mode using the full record of available coincident NILU irradiances (2.47 million  
 228 cases) to extract all vectors closest to local noon and within  $\pm 30$  minutes of the satellite overpass  
 229 time.  
 230 To calculate the uncertainty of the neural-network-based estimates of the retrieved erythemal dose  
 231 rates, the median absolute percentage error (MAPE) was calculated for the differences between the  
 232 NN estimates and the target values. Based on this statistical measure, we calculate that the

233 uncertainty of the NN in the dose rates was 3.6%, which is within the level of uncertainty of both  
 234 NILU and B086 irradiances which are 5.6% and 5% respectively. Taking the higher NILU  
 235 uncertainty as an upper bound on the radiance uncertainty and combining this in quadrature with the  
 236 NN uncertainty, we estimate the overall uncertainty on the NILU NN erythemal dose rate retrievals  
 237 to be 6.5%.

### 238 3.2. Comparisons of NILU-UV and UVB-1 erythemal data

239 To further verify the validity of the NILU NN erythemal retrievals, comparisons with the collocated  
 240 UVB-1 measurements were performed as an independent source of information. For these  
 241 comparisons, 1-minute synchronous NILU and UVB-1 data were used, while hourly mean values  
 242 were calculated in order to eliminate the influence of any possible time shifts and random  
 243 incidences (e.g. temporarily shading of the input optics) into the datasets. Additionally, hourly data  
 244 with more than 70% abundance in cloud-free minute measurements, as identified from the NILU  
 245 PAR algorithm (Zempila et al., 2016b), were characterized as “NILU clear skies”.

246 In Figure 1 the relative percentage differences between OMI and UVB-1 are presented for all and  
 247 cloud-free sky cases respectively. Although the distribution of the relative percentage differences is  
 248 normal, we provide the median and the 20-80 percentile values as measures of statistical  
 249 differences.



250 **Figure 1 (a)** Histogram of the relative percentage differences of hourly mean values for the NILU and UVB-1 erythemal dose  
 251 rates. Cases were more than 70% of the data were identified as cloud-free based on NILU PAR measurements, are indicated  
 252 in red. The median and 20/80 percentiles are also presented. **(b)** The SZA dependence of the relative percentage differences is  
 253 also depicted, along with the median percentage differences of 5°SZA bins. The error bars in the lower panel refer to the  
 254 20/80 percentile values.

255 As seen in Figure 1 (a), the overall conformity between the two ground-based datasets was quite

256 good with small median differences, -0.86% and 1.09% for all and cloud-free skies respectively, on  
257 a large number of coincidences (30506 for all skies, and 10108 for the NILU-based cloud free  
258 instances, as shown in Figure 1). Low values of the 20/80 percentiles were found within the  
259 uncertainty of both data sets; this shows that both time series result in comparable values.

260 To elaborate more on these comparisons, the influence of the SZA was also investigated (Figure  
261 1(b)). It was found that for SZAs less than  $70^\circ$  under cloud-free conditions the relative percentage  
262 differences resulted to a median of 0.45% with corresponding 20/80 percentiles of -3.25%/4.60%  
263 respectively. Furthermore, the SZA pattern seen in Figure 1(b) can be attributed to the different  
264 geometry of the input optics, differences in angular responses and calibration procedures applied to  
265 each dataset. For SZAs  $>70^\circ$  we observe larger scatter for both cloudless and clear sky cases as an  
266 impact of the non-ideal angular response of both instrument and the increasing signal to noise ratio.  
267 Summarizing, the comparisons of the NILU NN erythemal hourly doses revealed a good agreement  
268 with the collocated UVB-1 measurements. Therefore, the NILU NN erythemal data represent a  
269 valid dataset, with denoted uncertainty of 6.5% that is comparable with the uncertainty of the UVB-  
270 1 measurements.

271

#### 272 **4. Evaluation of OMI /Aura erythemal product**

273 In the following section, comparisons among the OMI and the NILU, UVB-1 and B086 erythemal  
274 data were performed. The OMI/Aura NASA algorithm provides erythemal dose rates at overpass  
275 time (measurement) as well as at local noon (interpolated). Both cases were investigated, while at  
276 the same time identification of cloud-free cases took place in two different ways: i) a cloud  
277 screening algorithm based on NILU-PAR measurements was used to define the NILU clear sky  
278 cases (NILU clear skies), according to Zempila et al., 2016b, and ii) the limitation of Lambertian  
279 equivalent reflectivity (LER) at 360 nm less than 0.1 was applied to satellite estimates in order to  
280 derive the satellite cloudless cases (OMI clear skies), according to Antón et al., 2010. Since most of  
281 the relevant studies use average values of 1 hour ( $\pm 30$ min) around the overpass time of the satellite  
282 (e.g. Chubarova et al., 2002), compensating in this way for moving clouds within the OMI pixel,  
283 the same statistics were recalculated for the 1 hour averaging as well. For the identification of the  
284 NILU cloud-free 1-hour averages, data within this timeframe with more than 70% cloud-free 1-  
285 minute measurements were characterized as hourly averages under clear skies (NILU clear skies).  
286 For the OMI clear skies, the same criterion, as above, was used (LER  $< 0.1$ ). In Table 3 we present a  
287 statistical summary of the comparisons performed for the overpass and local noontime, based on

288 both temporal matching approaches. For all comparisons, only satellite data within a radius of 50  
 289 km were taken into account, while comparisons within  $\pm 150\%$  were analysed to avoid including  
 290 erratic data (e.g. random drop of signal due to obscured ground sensor) into the statistics. The later  
 291 limitation ended to a 2.5% and 2.7% reduction of the original OMI/NILU and OMI/UVB-1 exact  
 292 overpass datasets respectively, while the reduction in the 1-hour overpass comparisons was 1.5%  
 293 for both OMI/NILU and OMI/UVB-1 comparisons. For the local noon comparisons, both  
 294 OMI/NILU and OMI/UVB-1 are reduced by 2.5% for the exact coincidences when limiting the  
 295 dataset within the range of  $\pm 150\%$ , while this limitation reduced the amount of coincidences of the  
 296 1-hour averages around local noon by 1.7% for both the two types of the ground-based instruments.  
 297 An overview of the backbone of this section is presented in **Table2** and Flow Chart 1, to facilitate  
 298 the readers.

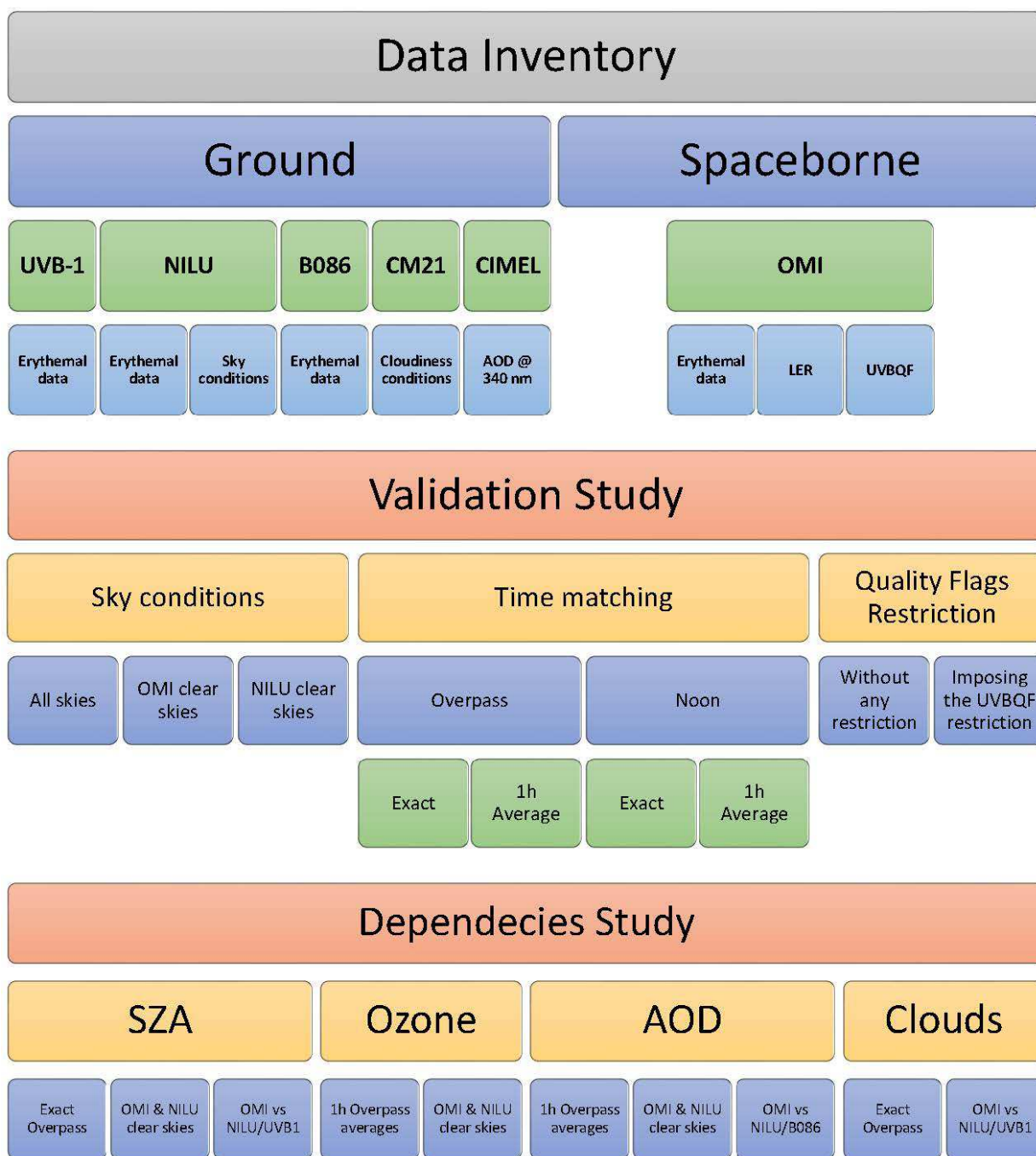
299

300 **Table2.** Overview of the measurement characteristics and datasets used in this study for the period  
 301 2005-2014 over Thessaloniki, Greece (lat: 40.69° N, lon: 22.96° E, alt: 60 m).

Instrument	Recording Frequency	Original Measurements	Derived Data	Cloud Information
Ground-based				
NILU-UV	1-min	Irradiances at 5 wv [ $\text{W}/\text{m}^2/\text{nm}$ ] PAR [ $\text{W}/\text{m}^2$ ]	Erythemal dose rates [ $\text{W}/\text{m}^2$ ] Cloud binary information	YES [using the PAR data]
UVB-1	1-min	Erythemal dose rates [ $\text{W}/\text{m}^2$ ]	Erythemal dose rates [ $\text{W}/\text{m}^2$ ]	NO
B086	20-40 min	Spectral irradiances [ $\text{W}/\text{m}^2/\text{nm}$ ]	Erythemal dose rates [ $\text{W}/\text{m}^2$ ]	NO
CM21	1-min	Solar radiation [ $\text{W}/\text{m}^2$ ]	Cloudiness information	YES
CIMEL	$\geq 15$ -min	unitless	AOD @ 340 nm	Cloud free cases
Spaceborne				
OMI	Daily	Erythemal dose rates [ $\text{W}/\text{m}^2$ ]	Erythemal dose rates [ $\text{W}/\text{m}^2$ ]	YES

302





303

304

305

**Flow Chart 1. Overview of the data inventory used in this study, along with a short description of the schematic of the validation and dependency studies performed between the ground- and satellite-based erythema data.**

306

307

308

309

310

311

The comparison statistics are presented in the form of median and 20/80 percentile values since the dataset cannot be represented with a normal distribution because the comparisons showed a persistent tendency towards higher relative percentage differences. In **Table 3**, for all skies at the exact overpass time, the agreement between the NILU and OMI erythema dose rates is 2.5% while the satellite overestimates by 4.1% at local noon, with a percentile range (80%-20%) of 24% and 11.2% respectively. Limiting the dataset to cloud-free cases based on OMI observations leads to

312 higher relative percentage differences, 4.0% for the overpass and 5.8% for the local noontime, with  
 313 the 20/80 percentile difference ranging between 11-12%. For the overpass comparisons, although  
 314 the median of the relative percentage differences seen under the NILU defined clear days is less  
 315 than the one referring to OMI clear skies cases, the later one presented lower scatter based on the  
 316 observed 20/80 percentiles. This was also the case when examining the noon values, where the  
 317 scatter seems to be marginally larger for the NILU clear results. The larger scatter in the noon  
 318 comparisons under all sky cases can be attributed to differences in the model/algorithm estimations  
 319 and differences in the geometry and type of the two sensors, since the OMI noontime values are  
 320 calculated through time extrapolation using the overpass time and assuming similar atmospheric  
 321 (cloud) conditions. Although the cloud-free cases result in lower amount of coincidences, the  
 322 median differences observed in OMI/NILU comparisons imply that the agreement of the OMI  
 323 erythemal dose rates is equally good under all-sky conditions as it is for the cloud-free cases.

324  
 325 **Table 3.** Statistical analysis of the differences between erythemal dose rates provided by OMI/Aura  
 326 and NILU/UVB-1/B086 for the exact overpass and local noontime coincidences. OMI/AURA data  
 327 are provided within a radius of 50 km from the site location. Differences with absolute values more  
 328 than 150% were eliminated.

	<b>Overpass</b>			<b>Local Noon</b>		
<b>(OMI-NILU)/NILU</b>	<b>All Skies</b>	<b>OMI Clear</b>	<b>NILU Clear</b>	<b>All Skies</b>	<b>OMI Clear</b>	<b>NILU Clear</b>
N counts	2013	691	761	2267	740	915
Median (%)	2.5	4.0	2.1	4.1	5.8	3.2
20/80 percentiles (%)	-8.5/15.5	-1.1/10.0	-4.7/8.4	-7.1/21.1	0.8/11.8	-4.4/9.4
<b>(OMI-UVB1)/UVB1</b>						
N counts	2009	691	761	2269	740	915
Median (%)	3.9	4.0	2.0	5.3	5.0	2.2
20/80 percentiles (%)	-7.7/22.5	-3.3/13.0	-6.1/10.3	-7.4/28.2	-1.9/14.7	-7.5/10
<b>(OMI-B086)/B086</b>						
N counts	43	14	18	162	63	69
Median (%)	4.5	4.7	4.4	4.9	6.3	2.9
20/80 percentiles (%)	-2.5/20.4	3.9/13.4	0.0/9.4	-4.8/16.7	-0.2/12.8	-4.4/10.4



329 Similarly, the OMI/UVB-1 comparisons revealed an agreement of 3.9% for the all skies cases  
 330 during the overpass time, which is slightly improved at 2% under the NILU defined clear cases,  
 331 while it remained unaltered at 4% for the OMI cloud-free limited dataset. The number of  
 332 coincidences was the same as for the OMI/NILU comparisons for both OMI and NILU cloudless  
 333 days. When analysing the local noon exact matching, the percentage differences were increased to  
 334 5.3%, 5.0% and 2.2% for all, OMI clear and NILU clear skies, and the number of coincidences was  
 335 also increased to 2269, 740 and 915 respectively. In general, the comparisons between OMI and  
 336 UVB-1 data at the exact overpass result in similar median differences with the OMI/NILU  
 337 comparisons, but the denoted percentile ranges are higher than the later ones. This aspect could be  
 338 an indicator on the uncertainty of the UVB- 1 erythemal dose rates, especially for high SZAs since  
 339 they are not corrected for the non-ideal angular response of the instrument.

340 OMI/B086 comparisons result in extremely few collocations for the exact overpass minute (43 for  
 341 the all skies cases), thus the statistical significance of the results is considered low, although the  
 342 percentages are not different from those of the OMI/NILU and OMI/UVB-1 differences. The low  
 343 number of coincidences during the satellite overpass is expected since B086 performs sky scans  
 344 within steps of 20 up to 40 minutes apart, making the existence of coincident overpass  
 345 measurements statistically rare. When checking the local noon exact coincidences, the number of  
 346 paired satellite and B086 data is almost quadrupled, 162, 63 and 69 for all skies, OMI clear skies  
 347 and NILU clear skies respectively, but still small to deduce a solid conclusion. It is though  
 348 reassuring that the results are similar to the ones obtained from the other comparisons, and as seen  
 349 in Table 3, for all cases and all comparisons, the NILU clear skies incidences provide the smallest  
 350 median value of the relative percentage differences, providing an additional means of verification of  
 351 the accuracy of the NILU data.

352

353 **Table 4.** Statistical analysis of the differences between erythemal dose rates provided by OMI/Aura  
 354 and NILU/UVB-1/B086 for the 1-hour average values around the OMI overpass and local noontime  
 355 ( $\pm 30$  minute). OMI/AURA data are provided within a radius of 50 km from the site location.  
 356 Differences with absolute values more than 150% were eliminated.

(OMI-NILU)/NILU	1h around Overpass			1h around Local Noon		
	All Skies	OMI Clear	NILU Clear	All Skies	OMI Clear	NILU Clear
N counts	2300	756	735	2298	755	774

Median (%)	3.9	4.8	2.8	5.6	6.6	4.6
20/80 percentiles (%)	-5.3/16.5	0.0/11.1	-3/8.6	-4.7/19.5	1.4/12.7	-1.8/10.4
<b>(OMI-UVB1)/UVB1</b>						
N counts	2300	756	735	2299	755	774
Median (%)	5.9	5.1	2.7	6.6	6.0	3.2
20/80 percentiles (%)	-4.9/22.8	-2.1/13.8	-5.1/10.3	-4.8/26.6	-0.9/15.3	-5.0/11.1
<b>(OMI-B086)/B086</b>						
N counts	1751	572	558	1448	485	523
Median (%)	6.9	7.1	4.6	5.2	6.1	3.7
20/80 percentiles (%)	-4.3/25.6	0.0/14.8	-2.9/12.2	-5.3/24.0	0.7/13.4	-1.7/11.1

357

358 When examining the 1-hour averaged values in Table 4, in all cases, apart from the B086 dataset  
359 (1751 coincidences instead of 1448 for all skies, 572 instead of 485 for the OMI clear skies and 558  
360 instead of 523 for the NILU cloud-free cases at the overpass and local noon respectively), the  
361 number of coincidences were similar between the 1 hour data around the overpass and the local  
362 noon. The median differences tend to show an enhanced overestimation by OMI for all cases (1h  
363 around overpass and local noon), for all and clear sky conditions, when compared to the exact time  
364 coincidences. On the other hand, the 20/80 percentile range seemed to be little affected by the  
365 temporal averaging of ground-based data, with the comparisons for the 1-hour averaged values to  
366 correspond in slightly smaller percentile ranges (~20%), again with the clear skies cases presenting  
367 the smaller range (12%-15%). As seen in the table, the 1-hour averaging favoured the number of  
368 coincidences under all skies cases in all comparisons with the ground-based instruments.  
369 Furthermore, the temporal averaging ended to smaller percentile ranges in most of the cases for  
370 both, exact and local noon, time matching. On the other hand, the median differences were slightly  
371 higher since OMI sees the pixel area at the exact overpass time, while the characterization of NILU  
372 cloud-free cases within 1 hour can result to different outcomes based on the limitation set on the 1-  
373 minute cloud-free cases (in our case a 70% abundance of cloud-free minute points was applied).  
374 Therefore, careful consideration of all available choices should take place based on the available  
375 data and the scope of each study, since exact overpass match and time averaging present their own  
376 benefits, while also introduce certain limitations.

377 To further investigate the accuracy of the OMI erythemal dose rates and since the OMI dataset also  
 378 provides additional information regarding the Quality Flags on Pixel Level (UVBQF), an analysis  
 379 on limiting OMI dataset based on the UVBQF was also performed. This 16 digits binary flag  
 380 elaborates on special characteristics for the quality of the OMI retrieved data and the input  
 381 information used in the satellite retrieval algorithm. For the UVBQF limitation, the usage of the  
 382 TOMS 380 nm monthly LER (MLER) climatology (Herman and Celarier, 1997) and the usage of  
 383 the moving time-window (MTW) climatology (Tanskanen et al. 2003) were permitted for the  
 384 surface albedo, along with the application of the aerosol correction.

385 Again the exact overpass and local noontime were examined (**Table 5**), while the potential of any  
 386 improvement on the comparisons by a time averaging, was also analysed in **Table 6**.

387

388 **Table 5** Statistical analysis of the differences between erythemal dose rates provided by OMI/Aura  
 389 and NILU/UVB-1/B086 for the exact overpass and local noontime coincidences when restrictions  
 390 on the UVBQFlags were imposed. Differences with absolute value more than 150% were  
 391 eliminated.

UVBQF Limited	Overpass			Local Noon		
	(OMI-NILU)/NILU	All Skies	OMI Clear NILU Clear	All Skies	OMI Clear NILU Clear	
N counts	947	277	322	1121	310	381
Median (%)	3.0	4.7	4.6	4.9	6.3	3.2
20/80 percentiles (%)	-8.6/17.7	-1.0/11.3	-5.1/8.4	-7.3/24.6	1.3/13.2	-3.8/9.7
<b>(OMI-UVB1)/UVB1</b>						
N counts	948	277	322	1122	310	381
Median (%)	5.1	4.5	2.0	6.8	6.1	2.2
20/80 percentiles (%)	-6.8/23.2	-2.7/13.9	-5.9/9.6	-6.4/32.1	-1.0/16.6	-6.2/9.8
<b>(OMI-B086)/B086</b>						
N counts	20	4	6	96	31	34
Median (%)	5.2	9.0	2.4	4.2	9.3	0.2
20/80 percentiles (%)	-1.2/38.2	1.3/15.1	-0.7/6.0	-7.0/15.4	-0.4/12.9	-9.4/9.8

392

393 Once again, the temporal averaging of 1-hour favoured the number of coincidences between

394 satellite- and ground-based data, while the UVBQF limitation results in a significant reduction of  
 395 the original coincidences. The quality flag that produced almost 36% reduction of the original OMI  
 396 dataset under all skies was the second in order UVBQF flag, which refers to data retrieved under  
 397 suspicious inputs into the radiative transfer model. For the limited dataset, the observed median  
 398 differences under all skies conditions denoted that the OMI local noon data, exact and 1-hour  
 399 averages, overestimate the NILU erythemal slightly more, by 4.9% and 5.8% respectively, when  
 400 compared with the values at the exact and 1-hour averages at the satellite overpass time (3.0% and  
 401 3.9% respectively). The same pattern was observed for the OMI/UVB-1 comparisons, though the  
 402 overestimation of the OMI data was found to be 5.1% and 6.4% for the exact and 1-hour averages at  
 403 the overpass time, compared to the respective 6.8% and 7.5% median differences of the noontime.  
 404 In general, the 20/80 percentile ranges are larger for the noontime values when compared with the  
 405 ones at the overpass for both NILU/UVB-1 and OMI comparisons (31.9% for the NILU and 38.5%  
 406 for the UVB-1), while the 1-hour mean values end to smaller range due to the time averaging,  
 407 27.2% and 34.3% respectively. Again, the 1-hour time averaging resulted in higher overestimation  
 408 in OMI retrieved erythemal dose rates, while it favoured the number of the paired satellite and  
 409 ground-based data. The percentile range was smaller for the time averaging case, meaning that the  
 410 compared data, OMI and NILU/UVB-1, presented less scattering than those that resulted from the  
 411 exact matching with imposing the UVBQF limitation. Since the UVBQF limitations did not  
 412 improve the comparison statistics and reduced significantly the number of coincidences on the exact  
 413 overpass, the application of such limitation should be carefully considered especially in cases where  
 414 the original dataset is limited in number.

415  
 416 **Table 6.** Statistical analysis of the differences between erythemal dose rates provided by OMI/Aura  
 417 and NILU/UVB-1/B086 the 1-hour averaged values around the OMI overpass and local noontime  
 418 ( $\pm 30$  minute). Differences with absolute value more than 150% were eliminated.

UVBQF Limited (OMI-NILU)/NILU	1h around Overpass			1h around Local Noon		
	All Skies	OMI Clear	NILU Clear	All Skies	OMI Clear	NILU Clear
N counts	1131	312	315	1151	315	332
Median (%)	3.9	5.5	2.3	5.8	7.1	4.5
20/80 percentiles (%)	-5.3/17	0.0/12.1	-4.2/8.8	-5.4/21.8	1.5/13.6	-2.6/10.9
<b>(OMI-UVB1)/UVB1</b>						

N counts	1132	312	315	1152	315	332
Median (%)	6.4	6.1	1.9	7.5	6.6	3.1
20/80 percentiles (%)	-4.8/24.6	-1.3/14.3	-5.1/9.6	-4.7/29.6	-0.1/16.6	-5.5/11.3
<b>(OMI-B086)/B086</b>						
N counts	857	248	241	708	206	223
Median (%)	7.9	8.3	4.7	5.6	6.8	3.7
20/80 percentiles (%)	-4.8/26.1	0.3/16.8	-3.0/13.1	-6.5/27.0	1.1/13.6	-2.1/11.2

419

420 For the cloud-free cases identified by OMI, the median value at the exact overpass was equal to  
 421 4.7%, while at the local noon the corresponding value is 6.3%. These numbers were slightly  
 422 improved to 4.5% and 6.1% for the UVB-1 comparisons. A similar behaviour was detected for the  
 423 1-hour average comparisons for the OMI clear cases, where the overestimation of the satellite  
 424 against NILU retrieved dose rates was 5.5% for the overpass and 7.1% for the local noon. The  
 425 corresponding values for the UVB-1 data were 6.1% and 6.6%. When imposing the cloudiness  
 426 characterization, the scatter of the coupled OMI/NILU data at the overpass, which is presented in  
 427 the 20/80 percentile form, was restrained to -1.0%/11.3% for the OMI clear cases to -5.1%/8.4% for  
 428 the NILU clear cases for the exact matching. However, the time averaging did not improve much  
 429 the interquartile range in the OMI/NILU comparisons.

430 Regarding the OMI/UVB-1 results, again the NILU defined clear cases resulted to lower median  
 431 differences and scattering for both overpass and local noontime exact time matching. The averaging  
 432 around the overpass time, similarly to the OMI/NILU comparisons, resulted to slightly higher  
 433 median values of the relative percentage differences, whereas the interquartile range of the results  
 434 was not improved drastically.

435 Although the OMI/B086 comparisons resulted in a smaller sample size, especially during the exact  
 436 time matching, the comparison results were in agreement with the comparison results using NILU  
 437 and UVB-1 data.

438

439 Based on these findings, we can conclude that imposing the UVBQF limitation to the original OMI  
 440 dataset did not significantly improve the comparison results. The number of coincident ground- and  
 441 satellite-based data was significantly reduced in all tested cases under the imposed limitation, while  
 442 the 1-hour averaging with UVBQF imposed limitations favoured the number of coincidences

443 between OMI and NILU/UVB-1 data when compared with the exact time matching. Similarly to  
444 previous findings, the scattering of the comparisons was generally less when applying the 1-hour  
445 time averaging, but the overestimation of OMI was a bit higher for this case.

446

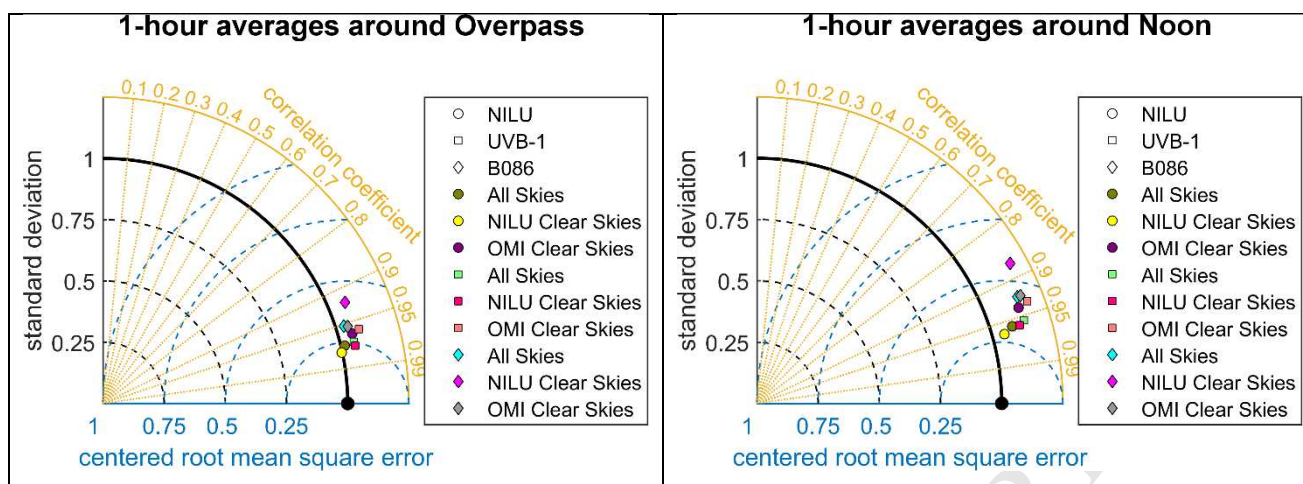
447 Summarizing, no significant deviations between the correlation statistics were seen in all tested  
448 combinations: exact overpass, exact local noon, 1-hour averages around the exact overpass and  
449 local noon, and the implementation of the UVBQF limitation on all previous combinations.  
450 Although cloud-free cases resulted in better correlation statistics, the all sky cases also presented  
451 low median differences as well, while the scattering of the comparisons was higher under all  
452 cloudiness conditions, as expected. In general, an overestimation of the OMI erythemal product by  
453 3-6% on average is expected when examining the overpass comparisons. For the noontime  
454 estimations, OMI seems to overestimate by 4-8%. Since the overpass time and the local noontime  
455 do not match (the mean visiting time over Thessaloniki is 11:45 UT, while the local noon is at  
456  $10:26 \pm 10$  UT), the noontime values are in practice projections of the overpass time values through  
457 model simulations based on the overpass atmospheric constituent retrievals, which can introduce  
458 higher uncertainty levels in the OMI retrievals.

459

460 To visualize the findings of the discussion above, normalized Taylor diagrams (Taylor, 2001) of the  
461 1-hour averages for each ground-based time series were produced for the overpass and noontime for  
462 all skies, NILU clear skies, and OMI clear skies without taking into account the UVBQF limitation  
463 that would lead to lower number of coincidences. OMI time series statistics were used as the  
464 reference dataset (black reference dot/line on Figure 2) for the shake of comparability between the  
465 different ground-based instruments.

466





467 **Figure 2** Normalized Taylor diagrams between OMI and NILU, UVB-1 and B086 erythemal dose rates for the 1-hour time  
 468 matching choice around overpass (left panel) and around noontime (right panel). OMI erythemal data were used as the  
 469 reference dataset (black dot on the diagrams), while the statistics of NILU data are presented as circles, UVB-1 data as  
 470 squares and B086 data as diamonds. The colours represent the cloudiness constriction imposed on each ground-based  
 471 dataset. Both standard deviations and centered root mean square errors were normalized to the standard deviation of the  
 472 reference dataset.

473 For the overpass comparisons in Figure 2 (left panel), both NILU and UVB-1 data under all  
 474 cloudiness conditions, showed high correlation coefficients ( $>0.95$ ) when compared with the  
 475 corresponding OMI dataset, while the standard deviations for most of the ground-based data were  
 476 found to be slightly higher than that of the OMI dataset, apart for the NILU data under the NILU  
 477 clear sky restriction. The centered root mean square error (CRMSE) is a means of measuring the  
 478 difference between the two compared datasets neglecting any observed bias between the two of  
 479 them. For the overpass comparisons, the normalized CRMSE ranged between 0.21 (for the  
 480 OMI/NILU comparison under NILU defined cloud free cases) and 0.41 (for the OMI/B086  
 481 comparison again under NILU defined cloud free cases).

482 For the noon comparisons provided also in Figure 2 (right panel), again the observed correlation  
 483 coefficients ( $R$ ) ranged between 0.94 and 0.96 apart for the comparisons performed for the  
 484 OMI/B086 datasets ( $R=0.93$  for all skies and OMI clear skies,  $R=0.88$  for NILU clear skies). In all  
 485 cases the normalized standard deviation was higher than the corresponding in the overpass  
 486 comparisons, denoting that for the noontime comparisons the ground-based data revealed higher  
 487 variability than the one corresponding to OMI noon values. Similarly, the CRMSE values were  
 488 higher than the ones for the overpass comparisons (0.21-0.41) further supporting the findings in

489 **Table 3.**

490

491 Based on these summary comments, we can conclude that each comparison scheme can be used to  
 492 serve specific purposes based on the scope of each study with equally well representation of the

493 statistical results. Overpass coincidences were proved to present better statistical results, since OMI  
494 measurements are taken at that particular time, while 1-hour averages of ground-based data around  
495 overpass time provided larger number of paired satellite- and ground-based erythemal data. Cloud-  
496 free cases, defined by the NILU PAR algorithm, provide a stricter limitation than OMI defined clear  
497 cases where the upper limit of  $LER < 0.1$  might result in clouds present within the OMI pixel. Users  
498 should also take into account the size of the final dataset, since as already discussed, specific  
499 limitations (cloudless skies, UVBQF limitation, limited BREWER datasets) can significantly  
500 reduce the amount of the paired satellite and ground data.

501

502 Since the differences between satellite and ground data are influenced by a set of parameters, like  
503 SZA, cloud optical thickness, ozone and AOD, in the following sections a thorough analysis is  
504 performed hoping to locate the main source of the observed discrepancies. For this evaluation, both  
505 exact and 1-hour averages around the overpass time were utilized, while the UVBQF limitation was  
506 not applied to avoid ending with a low number of coincidences.

507

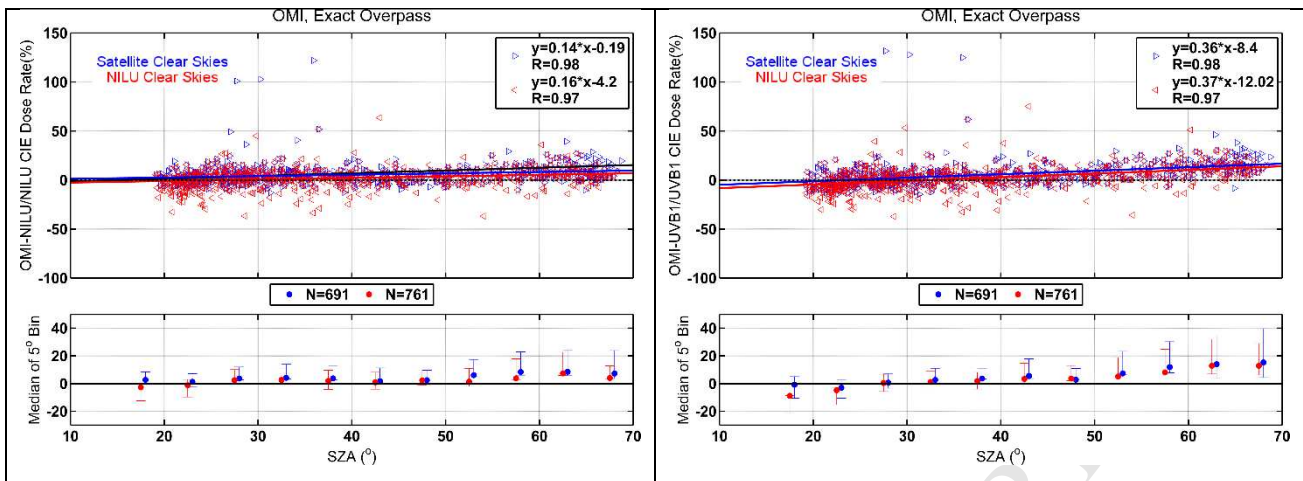
#### 508 **4.1. The SZA dependence**

509 For aerosol and cloud-free scenes and non-snow/ice surfaces the accuracy of the OMI erythemal  
510 dose rates depends mainly on the accuracy of the ozone column (OMI Algorithm Theoretical Basis  
511 Document III). The total root mean square (RMS) error is 3 % for a SZA of  $50^\circ$ , while this RMS  
512 error increases for increasing SZA and for shorter UV-B wavelengths. Thus, OMI erythemal  
513 retrieved values are expected to present a SZA dependence, with increasing uncertainties in higher  
514 SZAs.

515 In order to investigate the SZA dependence of the OMI dataset, the exact overpass time match was  
516 used to avoid discrepancies due to different SZA ranges within an hour between winter and summer  
517 periods. In Figure 3, the relative percentage differences between OMI and NILU (left panel), and  
518 OMI and UVB-1 (right panel) were plotted against the SZA at the time of the satellite overpass  
519 (upper panels). Median differences of  $5^\circ$  SZA bins were also investigated (lower panels), while the  
520 20/80 percentile range is also given in the form of error bars.

521





522 **Figure 3** SZA dependence of the relative percentage differences between the NILU and OMI erythemal dose rates (left panel)  
 523 **and the UVB-1 and OMI (right panel) at the exact OMI overpass time under cloud-free instances. Cases where the OMI LER**  
 524 **values are less than 0.1 are characterized as OMI Clear Skies and are depicted in blue, while data identified as cloud-free**  
 525 **based on NILU PAR measurements, are indicated as NILU Clear Skies and are depicted in red. The linear regression**  
 526 **equations are also displayed while the correlation coefficient  $\textcircled{R}$  between the original datasets OMI/NILU and OMI/UVB-1 is**  
 527 **also provided (upper panels). Median relative percentage differences of  $5^\circ$  SZA bins are presented along with the 20/80**  
 528 **percentile values depicted as error bars (lower panels).**

529 Based on Figure 3, left panel, there is no significant evidence of a SZA dependence between the  
 530 OMI and NILU estimates. When moving to higher SZA values, above  $55^\circ$ , the 20/80 percentile  
 531 range becomes wider even for the cloud-free data points, implying that at the higher observed solar  
 532 elevations, the two datasets present higher scattering that possibly led to an ascending small trend in  
 533 the slopes of the regression lines. On the right panel of the same figure, the exact same comparison  
 534 plots are given for the OMI and UVB-1 retrievals. For this later comparison, as seen in the lower  
 535 panel, there is a stronger SZA dependence for SZAs above  $50^\circ$ , with higher slopes, almost double  
 536 the slopes seen in the OMI/NILU comparisons, and lower y intersect values. This aspect could be  
 537 probably attributed to the UVB-1 dataset that was not corrected for its non-ideal angular response.  
 538 Still, all datasets present high correlation coefficients ( $>0.97$ ) in all cases, with the stronger  
 539 correlation observed under the satellite clear skies restrictions.

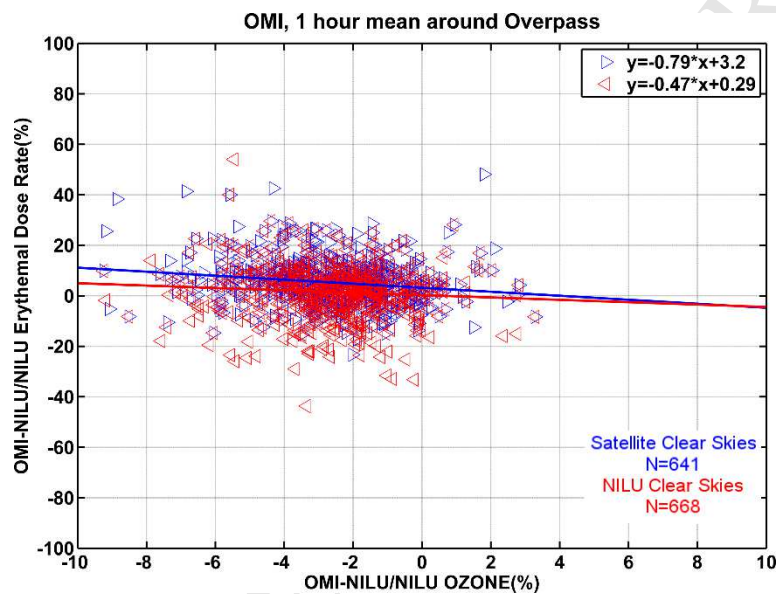
540 Generally, as seen in the lower panels of Figure 3, OMI erythemal values presented a relatively  
 541 small SZA dependence that resulted in higher overestimation of the product for SZAs above  $60^\circ$  for  
 542 the greater area of Thessaloniki, Greece; therefore, OMI data should be treated with caution for  
 543 SZAs exceeding  $60^\circ$ .

544

#### 545 **4.2.The Ozone dependence**

546 The validation study of the OMI total ozone columns (TOC) by Zempila et al. (2017a), proved that

547 on average OMI underestimates the TOC levels by ~2%. Since the OMI algorithm utilizes the TOC  
 548 information to derive the erythemal dose rates, the differences seen in TOC are expected to  
 549 influence the relative percentage differences of the retrieved values between the satellite- and  
 550 ground-based instruments. To explore the influence of the TOC, OMI TOMS TOC estimations  
 551 were compared against the NILU TOC values retrieved by a NN developed for this specific purpose  
 552 (Zempila et al., 2017a). In Figure 4, the relative percentage differences seen in erythemal dose rates  
 553 between OMI and NILU are plotted against the relative percentage differences in TOC between  
 554 OMI and NILU under cloud-free cases for the 1-hour averages around the OMI overpass time.  
 555



556  
 557 **Figure 4 Erythemal relative percentage differences between OMI and NILU data against TOC relative percentage**  
 558 **differences again between OMI and NILU. The linear least square fits are also presented. The comparisons are performed**  
 559 **only for cloud-free cases for the 1-hour averages around the OMI overpass time using the OMI cloud restriction (LER<0.1)**  
 560 **and the NILU PAR based cloud restriction (Cloud-free 1-minute data>70%).**

561 For the comparisons between OMI and NILU presented in Figure 4, most of the differences seen in  
 562 the TOC values lying within  $\pm 3\%$  (x-axis range). As expected, when OMI TOMS TOC values are  
 563 less than the corresponding retrieved by NILU measurements, OMI is higher than the NILU derived  
 564 ones. This fact results to descending slopes for both OMI and NILU defined cloud-free skies that  
 565 were proved statistically significant via F-test (stronger significance was seen in the satellite clear  
 566 skies cases where the p value was of the order of  $10^{-5}$ ) performed on the datasets. In general, a mean  
 567 underestimation of 2% in TOC by OMI under cloud-free conditions, as stated by Zempila et al.  
 568 (2017a), can lead to an average overestimation in the OMI data of 1% to 5%, for the NILU clear  
 569 skies and OMI clear skies respectively. Consequently, users are suggested to bear in mind that a

570 part up to 5% of the overestimation in OMI data could be introduced from deviations seen in OMI  
571 TOC retrieved values under clear skies.

572

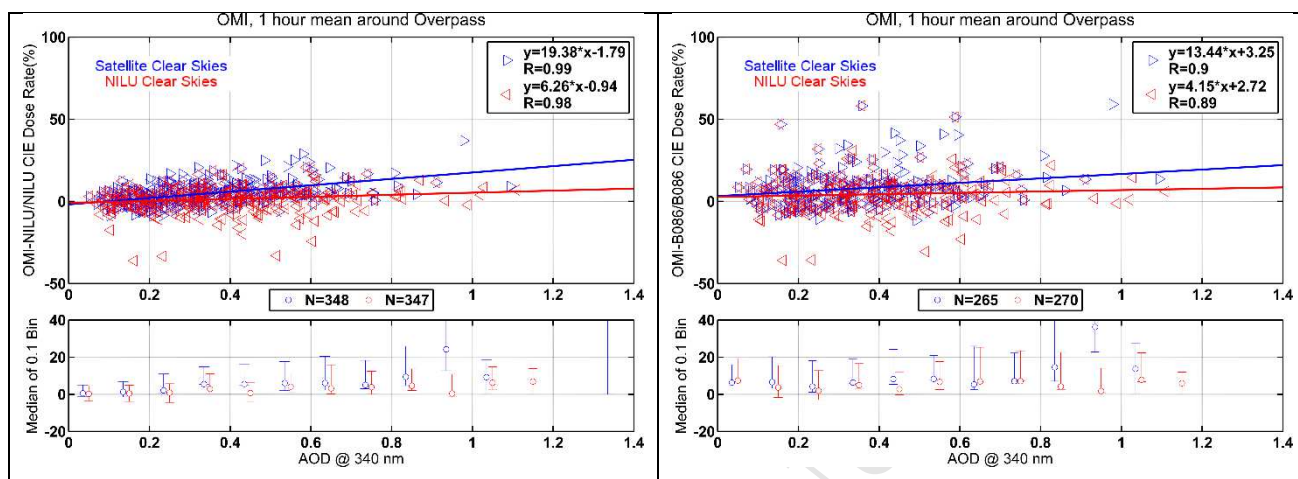
### 573 **4.3. The Aerosol dependence**

574 Due to the imperfect knowledge of the optical properties of the aerosols, non-absorbing and  
575 absorbing ones, and pollutants in the boundary layer, the retrieval of the OMI UV products is  
576 limited and the comparisons with ground-based data are expected to be influenced by deviations of  
577 AOD from the values that OMI uses to derive its UV products (Arola et al., 2009).

578 To investigate the effect of aerosols in the observed relative differences between satellite- and  
579 ground-based erythemal data, aerosol optical depths at 340 nm from the CIMEL sunphotometer that  
580 operates in Thessaloniki, were also used (Balis et al., 2010). According to Kazadzis et al. (2007),  
581 aerosol optical depths in UV experience a seasonal variation in Thessaloniki, with higher AOD  
582 values at 340 nm retrieved in August and lower values in December. Furthermore, in Thessaloniki,  
583 the aerosols are a contribution of marine, mineral dust and anthropogenic sources that make the  
584 aerosol scene more complex. In the same study, back trajectories proved that additionally to local  
585 aerosol sources, transport of aerosols takes place, especially during the summertime. It was proven  
586 that air masses coming from the North and North Eastern directions result in high aerosol loads over  
587 Thessaloniki, while minimum AOD is associated with air masses originating from the Atlantic  
588 Ocean. These findings clearly denote that in Thessaloniki the aerosol optical depths are a result of a  
589 rather complex mixture that makes the AOD retrieval by space-born instruments a non-trivial task  
590 (Koukouli et al., 2006).

591 CIMEL provides measurements of aerosol optical depths since 2011, thus only 4 years of  
592 measurements were available for this evaluation. Again, the datasets were distinguished into two  
593 categories, one comprising for the cases were the OMI detected LER values below 0.1, while the  
594 second set only included measurements during which the NILU cloud detection algorithm resulted  
595 into more than 70% cloud-free moments within the hour around the overpass. In order to increase  
596 the data points, 1-hour averages around the overpass time were taken into account, while the NILU  
597 and B086 data were used to minimize any influence of the SZA dependence seen in the OMI/UVB-  
598 1 comparisons (Figure 3). Although the statistical sample is small, OMI erythemal dose rates  
599 showed a slight dependence on the aerosol load at the site, especially in high AOD values, in both  
600 discriminations of cloudless cases and comparisons; OMI/NILU is shown in Figure 5 (left panels)  
601 and OMI/B086 in Figure 5 (right panels). This behaviour can probably be attributed to the way that

602 the correction on OMI UV irradiances is performed based on monthly AOD and SSA climatology  
 603 at 315 nm (Arola et al., 2009), that probably cannot interpret high aerosol loads at the station.  
 604 Cases with more than 0.7 AOD cover for the OMI cloud-free skies occupied 3.2% of the total  
 605 dataset, while under the NILU cloud-free limitation this percentage augmented to 6%.  
 606



607 **Figure 5** Erythemal relative percentage differences between OMI and NILU (left panel), and OMI and B086 (right panel)  
 608 data against AOD estimations from a CIMEL sunphotometer at 340 nm. The least square linear fits are also presented, while  
 609 the correlation coefficients between the OMI/NILU and OMI/B086 datasets are also depicted (upper panels). The median  
 610 relative percentage differences of the relative erythemal dose rate differences within 0.1 bin of AOD are provided in the lower  
 611 panels, while the 20/80 percentiles are depicted as error bars. The comparisons are performed only for cloud-free cases for  
 612 the 1-hour averages around the OMI overpass time using the OMI cloud restriction (LER<0.1) and the NILU PAR based  
 613 cloud restriction (Cloud-free1-minute data>70%).

614 Based on the findings in Figure 5 (left panel), under the NILU defined cloud-free cases, the average  
 615 overestimation of the OMI erythemal dose rates is  $\sim 6.3\%$  per AOD at 340 nm unit. Since the  
 616 average AOD at 340 nm during the examined period is  $0.43 \pm 0.25$ , the expected average percentage  
 617 overestimation of OMI values is  $2.8\% \pm 1.6\%$ . This number was tripled when examining the OMI  
 618 cloud-free cases. Similar behaviour was observed for the OMI/B086 comparisons, but smaller  
 619 slopes were obtained, verifying that OMI tends to overestimate the erythemal dose rates for cases  
 620 where high aerosol loads were measured at Thessaloniki. It should be also highlighted that the  
 621 OMI/NILU comparisons presented high correlation coefficients ( $>0.98$ ) in all cases, while the  
 622 OMI/B086 comparisons showed lower correlation coefficients mainly due to the way that the time  
 623 match was performed due to the smaller number of B086 spectra measurements.

624 Nevertheless, the obtained comparisons showed better agreement between OMI and ground-based  
 625 measurements than the one revealed by Kazadzis et al. (2009) since the OMI algorithm currently  
 626 corrects the UV products for absorbing aerosols based on the study by Arola et al. (2009). Users

627 could combine the information provided by OMI regarding the retrieved AOD values in order to  
 628 assess the accuracy of OMI erythemal product and/or apply an upper cut-off limit to achieve better  
 629 agreement between ground- and satellite-based erythemal values.

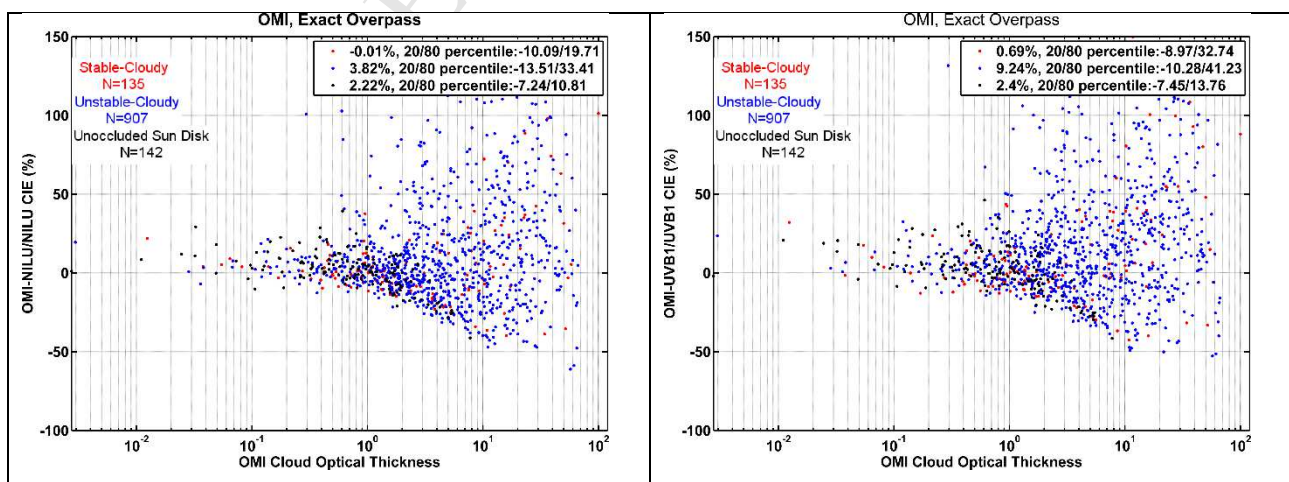
630

631

#### 632 4.4. The Cloud dependence

633 Since the OMI algorithm interprets clouds as a uniform cover over the pixel, an analysis on the  
 634 effect of clouds should take place in order to evaluate the performance of the satellite algorithm  
 635 under various cloudiness conditions. As mentioned before, OMI provides an estimation of the COT  
 636 seen within the pixel at the exact overpass time. In addition, the study by Vasaras et al. (2001) uses  
 637 8-minute averages of 1-minute measurements of GHI from a CM21 pyranometer that is operating at  
 638 LAP/AUTH since 1993, to determine whether the measurement was taken under stable or unstable  
 639 cloudy conditions or under unoccluded sun disk. In order to investigate the influence of the clouds  
 640 on the relative differences, overpass exact time matching data (coincidence within one minute)  
 641 under all skies conditions were used. The sun disk coverage information provided by the CM21  
 642 cloud description algorithm introduced by Vasaras et al. (2001), was also included into the  
 643 comparisons. Based on the algorithm, cases where the sun disk was completely covered by clouds  
 644 were identified as “stable-cloudy” conditions, while “unstable-cloudy” conditions stated the state  
 645 where the sun was partially covered by clouds. The cases where clouds were present in the horizon  
 646 and were identified by the NILU PAR cloud-screening algorithm, but the CM21 algorithm resulted  
 647 to unobstructed sun disk were identified as “unoccluded sun disk” instances. Results of the  
 648 comparisons under these three cloud identified circumstances, are shown in Figure 6.

649



650 Figure 6 Relative percentage differences of the OMI and NILU (left panel), and OMI and UVB-1 (right panel) derived

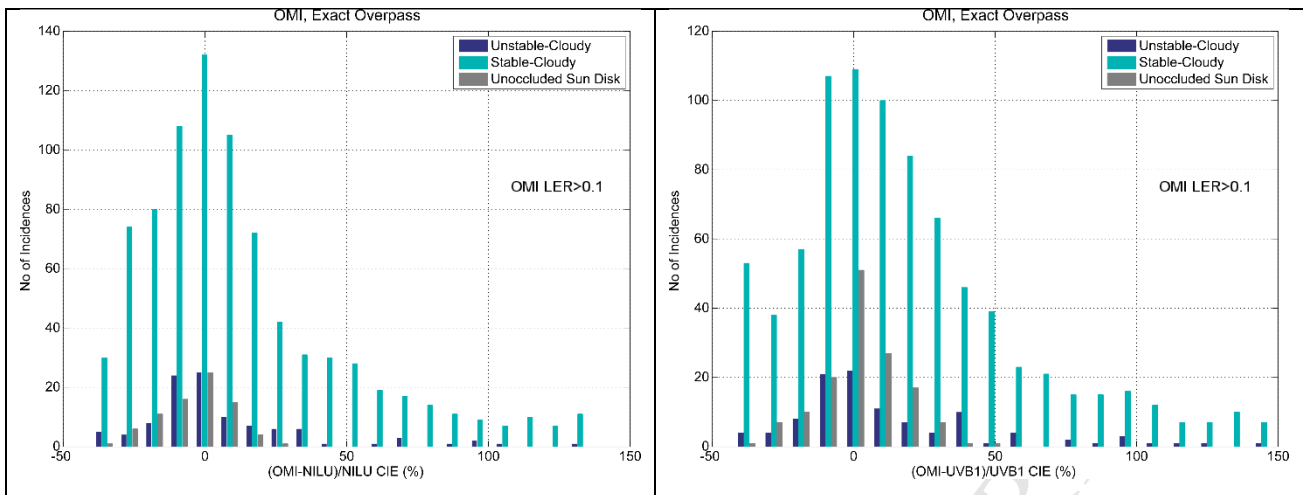


651 erythema dose rates are presented at the exact overpass time against the COT values reported by OMI in a logarithmic x-  
652 axis (upper panels). Three cases were distinguished based on the CM21 cloud-flagging algorithm: (i) Stable-Cloudy  
653 conditions during which the sun disk is completely obscured, (ii) Unstable-Cloudy conditions during which the sun disk is  
654 partially covered by clouds, and (iii) Unoccluded sun disk during which NILU PAR algorithm detects clouds while the CM21  
655 algorithm reports unobscured sun disk. Median differences along with the 20/80 percentile range are also depicted.

656 As seen in both panels of Figure 6, the discrepancies between the two sets, ground- and satellite-  
657 based, become higher with higher cloud optical thicknesses seen by the satellite sensor that could be  
658 attributed to the fact that at higher COT values, irradiances are too low resulting to higher relative  
659 percentage differences. Since OMI receives backscattered irradiances from an area between  $13 \times 24$   
660  $\text{km}^2$  in the nadir to  $24 \times 102 \text{ km}^2$  on the edges of the OMI swath, the optical geometry is significantly  
661 different from the single point measurements that NILU and UVB-1 perform. The presence of  
662 scatter clouds over the horizon can lead to complicate radiation scenes that are impossible to  
663 capture by nadir-viewing satellite measurements. For larger COT values, the scene seen in both  
664 OMI/NILU and OMI/UVB-1 comparisons was rather complicated, with cases where OMI  
665 underestimated (negative relative percentage differences) and cases where OMI overestimated  
666 (positive relative percentage differences). For both panels in Figure 6, there was an unequal spread  
667 of the percentage differences, where cases during which OMI overestimated resulted in higher  
668 comparison numbers ( $>50\%$ ), while the cases during which OMI underestimated the erythema dose  
669 rates resulted in relative differences greater than  $-50\%$ . This fact, along with the fact that the  
670 number of points with positive relative percentage differences, 1191 for the OMI/NILU comparison  
671 and 1234 for the OMI/UVB-1 respectively, was larger than the one with negative differences, 822  
672 for the OMI/NILU and 755 for the OMI/UVB-1 comparisons respectively, led to an average  
673 overestimation in OMI retrievals.

674 To further investigate this aspect, histograms of the relative percentage differences were examined  
675 for the 3 cloudiness conditions where the LER values reported by OMI were more than 0.1  
676 ( $\text{LER} > 0.1$ ), in order to verify that the OMI was also seeing clouds into the pixel.

677



678 **Figure 7** Histograms of relative percentage differences between OMI and NILU (left panel), and OMI and UVB-1 CIE (right  
 679 panel) dose rates for three cloudiness conditions (as described in Figure 6). The results are presented for cases where the  
 680 OMI LER values were more than 0.1 (LER>0.1).

681 The histograms in Figure 7 revealed distinct patterns among the three cloudiness condition groups  
 682 that are consistent in both NILU/OMI and UVB-1/OMI comparisons. Under a partially covered sun  
 683 disk (unstable cloudy conditions), both distributions in the left and right panel of the figure, are  
 684 wide, with low count numbers, while OMI seems to underestimate the NILU erythemal dose rates  
 685 since the majority of the points were piled into the negative relative percentage difference area (left  
 686 panel). This behaviour could be partially attributed to the fact that OMI treats clouds as  
 687 homogenous while it assumes that they cover the whole pixel of interest. Thus, when direct  
 688 radiation is present, OMI tends to underestimate the erythemal values. Furthermore, a weak  
 689 secondary peak seemed to be present in the OMI/UVB-1 comparisons under unstable cloudy  
 690 conditions (right panel of Figure 7) leading to higher number of positive percentages, probably due  
 691 to SZA dependencies as discussed to a previous section (Section 4.1) and/or low area of unobscured  
 692 sun disk.

693 When limiting the datasets to instances where the sun was completely covered by clouds (stable  
 694 cloudy conditions as they are referred to in Figure 7), the distribution is quite wide and skewed  
 695 towards positive relative differences, which declares that OMI overestimates the corresponding  
 696 ground-based values for most of these cases. Furthermore, again in OMI/UVB-1 and possibly in  
 697 OMI/NILU comparisons, there is a secondary weaker peak implying that under certain conditions  
 698 when the sun disk is completely covered, OMI tends to overestimate the erythemal dose rates by  
 699 45% or more. In this occasion, the exact position of the station does not interfere with the results,  
 700 since the diffuse radiation dominates during these cloudiness conditions, something that is not the  
 701 case for the other two classified groups (unstable cloudy and unoccluded sun disk). An

702 underestimation of the cloud optical thickness by OMI could lead to higher erythemal retrieved  
703 rates than the corresponding ground-based values.

704 For the cases under which the sun was uncovered, the distribution of the percentages is narrower  
705 when compared to the other two cloudiness cases, and the peaks were approaching zero percentage  
706 values for both the OMI/NILU and OMI/ UVB-1 comparisons. For these occasions, one would  
707 expect the OMI to retrieve in general lower erythemal values than the real ones, since the retrieval  
708 algorithm assumes that clouds cover the whole pixel, while an unoccluded sun disk would result in  
709 higher direct irradiances and thus higher erythemal values.

710 Although the major difference between these comparisons results from the fact that OMI  
711 measurements represent the mean surface erythemal dose rates over a wide region rather than at a  
712 point as is the case with ground-based data. In such comparisons, OMI tends to overestimate the  
713 erythemal dose rates under cloudy conditions. However, very large differences revealed for very  
714 high COTs (>10) in figure 6, are linked with GHI attenuation on the order of ~300% compared with  
715 cloudless skies. Therefore, these differences were affecting the statistical evaluation but in practise,  
716 they were differences seen during very low irradiance levels. OMI data users are encouraged to  
717 examine thoroughly the cloudiness information provided by OMI (LER, COT) in order to  
718 concatenate accordingly the dataset based on their study purposes.

719

#### 720 **4.5. The UV index comparisons**

721 Although UV index (UVI) and erythemal data are expressions of the same biological parameter -  
722 the erythema of the human skin when exposed to UV solar radiation - in most health related studies,  
723 the UV index is the common parameter describing the effects of exposure to solar UV radiation  
724 (WHO, WMO, UNEP, ICNIRP, 2002; Lucas et al., 2006; Eide & Weinstock, 2005; Gonçalves et  
725 al., 2011; among others). The instant UVI is in fact the erythemal dose rate (in  $W/m^2$ ) multiplied by  
726 40 (Vanicek et al., 1999; WHO, WMO, UNEP, ICNIRP, 2002). This measure was first formulated  
727 in Canada to result to a maximum value of 10 at that region, while it was adopted by the World  
728 Meteorological Organization 2 years later, in 1994 (WHO, WMO, UNEP, ICNIRP; 2002, Fioletov  
729 et al., 2010) as a means of an easier interpretation of the UV exposure risks and rise of public  
730 awareness.

731 Nowadays, NASA's Earth data webpage ([https://earthdata.nasa.gov/earth-observation-data/near-  
732 real-time/download-nrt-data/omi-nrt](https://earthdata.nasa.gov/earth-observation-data/near-real-time/download-nrt-data/omi-nrt)) provides OMI UVI data in near real-time (average latency:  
733 100-165 minutes which is expected to be reduced in near future), thus supporting the efforts for



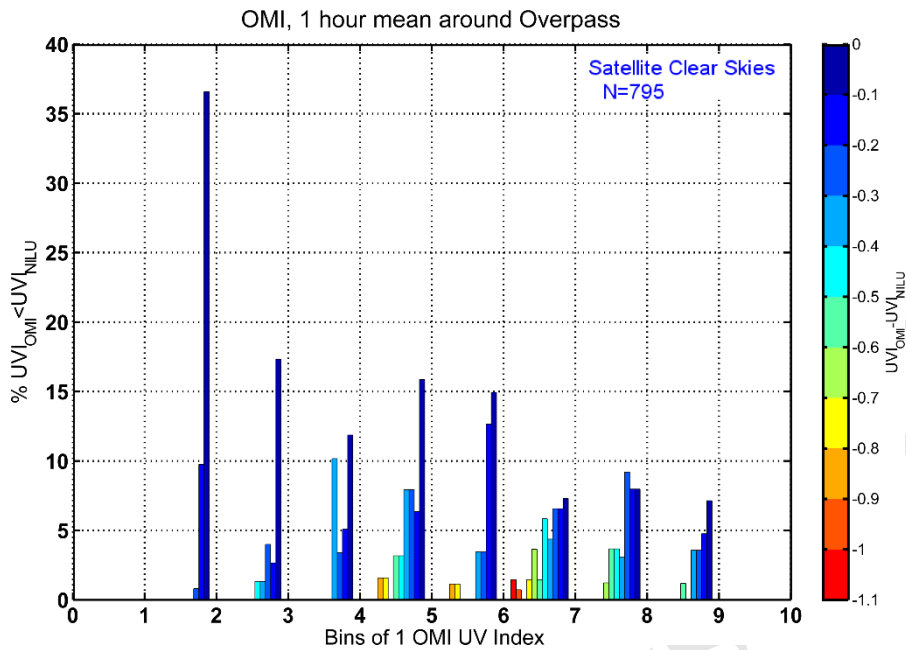
734 timely distribution of data related to earth observation, environment protection and public  
735 awareness.

736 Since for health studies the higher values of UVI are of most importance during which the impact of  
737 solar UV exposure is more immense, the study focused on the cases where the OMI UVI was lower  
738 than the NILU detected one. Among the ground-based available measurements, the NILU data were  
739 chosen to depict this aspect due to better statistic results (Section 4). Here only the discrimination  
740 between satellite cloud-free cases ( $LER < 0.1$ ) was imposed onto the datasets since this information  
741 is available to all data users, while the 1-hour mean values around the overpass time were  
742 investigated to maximize the number of coincidences.

743 To depict this aspect relative percentages (Number of cases where  $UVI_{OMI} < UVI_{NILU}$  over the total  
744 number of coincidences within the OMI UVI bin) for each OMI UVI bin of 1 unit width were  
745 plotted in Figure 8. The differences between the UVIs, OMI and NILU, were classified in  
746 differences of 0.1 as presented in the colour bar of Figure 8. For the “Low ( $UVI < 3$ )” UVI levels,  
747 OMI underestimated up to 10% the UVI values, but for these cases the impact on humans and  
748 ecosystems is low due to the low intensity of the UV radiation. For the moderate UVI range  
749 ( $3 \leq UVI < 6$ ), OMI had a maximum underestimation of 0.9 when compared to the NILU UVI for the  
750 bins of 4-5 and 5-6. This would not affect the set alerts on the UVI levels, since even with this  
751 underestimation the OMI derived UVI would result in the moderate UVI classification. For the high  
752 UVI levels ( $6 \leq UVI < 8$ ), the differences observed in the 6-7 OMI UVI bin could lead to a false  
753 indication of moderate UVIs, since differences between 0.9 and 1.1 were observed. However, these  
754 cases only occupy 2% of the points in this particular bin. For the adjacent bin of 6-7 OMI UVIs,  
755 although differences can reach up to -0.6 with OMI underestimating, the outcome UVIs would be  
756 still characterized as high, thus the proposed protection measures for this level of UVIs would not  
757 be altered. The same applied to the characterized as high UVIs (8-10), where the maximum  
758 underestimation was -0.6 in the 8-9 bin. Although this underestimation in OMI UVIs is relatively  
759 high, it would not affect the alert on the UVI levels since it would result to a high UVI  
760 classification.

761 Thus, we can conclude that OMI UVI values are reliable when concerning the characterization of  
762 the ambient UV radiation impact as low, moderate, high and very high in the greater area of  
763 Thessaloniki for the period 2005-2014 under cloud free skies where the impact of exposure to solar  
764 UV radiation is more intense.

765



766

767

768

769

Figure 8 Percentages of the number of cases where OMI UVIs were found to be lower than the corresponding NILU UVI for each bin of 1 OMI UVI under the OMI defined clear skies. Within each OMI UVI bin the difference between the two UVIs, OMI and NILU, are depicted in different color bars.

770

771

## 5. CONCLUSIONS

772

773

774

775

In this study ground-based measurements, model estimates, and satellite retrievals of CIE effective dose rates have been formed, compiled and associated to thoroughly analyse their accuracy at the mid-latitude UV and Ozone monitoring station in the Laboratory of Atmospheric Physics of the Aristotle University of Thessaloniki, Greece.

776

777

778

779

780

781

782

783

A NN was trained on NILU-UV multi-filter radiometer irradiance data at 5 different UV wavelengths together with collocated spectra from a Brewer MKIII spectrophotometer to produce 1-minute time series of erythemal dose rates. Furthermore, the NN erythemal dose rates were compared with UVB-1 measurements at the same temporal resolution (1 minute) to provide the level of agreement between the two ground-based datasets. The comparisons between the mean hourly values between the UVB-1 and NILU CIE dose rates revealed a good agreement of 0.86% under all skies with 20/80 percentiles within the uncertainty of the original measurements themselves.

784

785

786

In the context of space born CIE dose rates, estimates from the OMI/Aura instrument were used. The NASA Aura Data Validation Center provides overpass files including the OMI global attributes and geolocation along with all instrument data fields. Under the data fields subsection, the

787 erythemal dose rates are provided at the exact overpass time and at the solar local-noon along with  
788 the UV algorithm quality flags (UVBQF) and the UVI values. For all the comparisons performed in  
789 this study, satellite collocations within a radius of 50 km from Thessaloniki were taken into  
790 account, while differences of absolute value of 150% and more between satellite and ground  
791 erythemal data were omitted.

792 The comparisons of the ground products with the satellite retrievals revealed the following major  
793 points:

- 794 • For the nominal comparisons at the exact overpass time, OMI erythemal dose rates  
795 overestimated the NILU-UV retrieved values by 2.5%, while this difference was increased to  
796 3.9% when compared to the UVB-1 data. Under cloud-free cases detected by the PAR cloud  
797 binary detection algorithm, the percentage of the OMI overestimation fell to ~2% for both  
798 NILU-UV and UVB-1 comparisons.
- 799 • For the local noon exact comparisons, OMI presented higher erythemal dose rates of about  
800 4.1% when compared to NILU, slightly higher at 5.3% for the OMI/UVB-1 comparisons.  
801 When limiting the data set to cloud-free cases, the agreement between the satellite and ground-  
802 based estimates was improved, with relative percentage differences between 2-3% for the  
803 NILU-defined cloud-free cases.

804 In order to compensate for the OMI footprint and for any changes in cloud position and optical  
805 properties, 1-hour averages around the overpass time were also considered.

- 806 • The time averaging favors the number of coincidences by a 15% increase. Under all sky cases,  
807 OMI overestimated on average the erythemal dose rates at the overpass time by 3.6% when  
808 compared to NILU and by 6.6% when compared to UVB-1 data. Higher relative percentage  
809 differences were seen when OMI data were related to B086 estimates (~7%). These numbers  
810 were decreased when the under investigation datasets were limited to cloud-free skies: 2.8%,  
811 2.7% and 4.6% for the OMI/ NILU-UV, UVB-1 and B086 comparisons respectively.
- 812 • The time averaging of 1-hour around the solar local-noon time under all sky conditions, had not  
813 major impact on the comparisons between OMI and NILU-UV and B086. When limiting the  
814 original datasets based on the PAR cloud-screening algorithm, the relative percentage median  
815 values were found to lie within the range of 3-4.5%.

816 For the comparisons performed, the limitation of the OMI data based on the UVBQF was also  
817 investigated:

- 818 • The imposed limitation decreased the available dataset by almost 36%, while it did not  
819 significantly improved the comparison statistics of any of the above-mentioned schemes: exact  
820 and 1-hour averages around overpass and solar local noontime, and cloudiness conditions.

821  
822 In general, all comparison schemes (different ground-based instruments, averaging practices,  
823 comparison limitations) presented similar, moderate relative percentage differences, with OMI CIE  
824 data being higher than the corresponding ground-based. In more details:

- 825 • Overpass comparisons resulted in better comparative statistics than the noon comparisons,  
826 since OMI estimates its noontime UV products based on the measurement performed at the  
827 overpass without taking into account changes in ozone, aerosols and clouds.
- 828 • Cloud-free cases defined by the NILU PAR algorithm provided a more strict limitation than the  
829 OMI defined clear cases where the upper limit of  $LER < 0.1$  might result in clouds present  
830 within the OMI pixel.

831  
832 Seasonal effects in the satellite estimates were also investigated through SZA, ozone, aerosols and  
833 cloud dependences of the relative percentage differences between OMI and ground-based  
834 measurements.

- 835 • OMI CIE retrieved values are expected to present a SZA dependence for SZAs above  $50^\circ$  due  
836 to higher uncertainty in the ozone retrievals. The comparisons between OMI and NILU-  
837 UV/UVB-1 data, showed a tendency of OMI to overestimate CIE dose rates for SZA above  
838  $60^\circ$ , which was obvious for both all and cloud-free skies.
- 839 • A mean underestimation in OMI TOC values by 2% under cloud-free conditions led to an  
840 overestimation of 1% to 6% in the OMI CIE data under clear skies cases.
- 841 • Compared to the Kazadzis et al. (2009) study, the results presented here were improved due to  
842 the aerosol correction applied to all UV products based on Arola et al. (2009). On average OMI  
843 overestimated by  $\sim 6.5\%$  per aerosol optical depth (AOD) at 340 nm unit when compared to  
844 NILU data. The average AOD at 340 nm during the examined period was  $0.43 \pm 0.25$ , therefore  
845 the expected average percentage overestimation of OMI CIE values due to imperfect aerosol  
846 treatment in the algorithm is  $2.8 \pm 1.6\%$ .

847  
848 Since OMI algorithm treats clouds as a uniform layer over the entire pixel, different types of  
849 cloudiness were investigated based on the stable cloudy (fully covered sun disk), unstable cloudy

850 (partially covered sun disk) and unoccluded sun disk indications acquired by the CM21 based  
851 algorithm.

- 852 • In general under high COT values the discrepancies observed between the satellite- and  
853 ground-based were higher due to low values of absolute irradiances.
- 854 • For the cases where stable cloudy conditions were identified (fully covered sun disk), OMI had  
855 the tendency to overestimate the ground-based CIE data.
- 856 • For the unstable cloudy conditions (partially covered sun disk), the exact opposite pattern was  
857 observed, with OMI data underestimating in general the ground-based erythemal dose rates.
- 858 • When the CM21 algorithm detected unoccluded sun disk under cloudy conditions, OMI CIE  
859 retrievals presented a narrow distribution around zero relative percentage differences, without  
860 any obvious preference towards positive or negative values for both NILU and UVB-1  
861 comparisons.

862

863 As the UVI is a mean of alerting the public on harmful effects when exposed to solar UV radiation,  
864 OMI overpass UVI data were also validated through NILU estimates:

- 865 • OMI UVIs provided higher estimates than the ground-based UVIs in most of the classifications  
866 of UVI based alert zones (low, moderate, high, and very high).
- 867 • For the cases where OMI UVIs were found to be lower than the NILU retrieved ones, no  
868 significant impact on the above mentioned classifications was observed.

869 Therefore, the UVI classification under cloud-free conditions based on OMI estimates can be used  
870 to alert public awareness in the greater area of Thessaloniki.

871

872 In conclusion, this comprehensive work elaborated on the accuracy of ground- and satellite-based  
873 estimates of erythemal UV dose rates and UVI values, revealing the merits but also the constraints  
874 of the methods applied to both type of datasets. Since space-borne data provide global coverage,  
875 their UV products can be used to increase awareness of the harmful effects of overexposure to UV  
876 radiation and alert public when necessary. Therefore, we believe that such studies are of high  
877 importance in order to provide insight regarding future missions and facilitate potential  
878 improvements of the future generation of UV measuring space born sensors.

879

880

881 Acknowledgements: The Dutch-Finnish built OMI instrument is part of the NASA EOS Aura satellite payload. The

882 OMI project is managed by NIVR and KNMI in the Netherlands. We thank the OMI International Science Team for the  
883 satellite data used in this study. The authors would also like to acknowledge the National Network for the Measurement  
884 of Ultraviolet Solar Radiation, [uvnet.gr](http://uvnet.gr).

ACCEPTED MANUSCRIPT

## REFERENCES

- 886 1. A Jebar, M.A., Parisi, A.V., Downs, N.J., and Turner, J.F., 2017. Validation of Ozone  
887 Monitoring Instrument UV Satellite Data Using Spectral and Broadband Surface Based  
888 Measurements at a Queensland Site. *Photochemistry and Photobiology*, 93, 1751-1097.
- 889 2. Allaart, M.,M. van Weele, P. Fortuin and H. Kelder, 2004. An Empirical model to predict the  
890 UV-index based on Solar Zenith Angle and Total Ozone. *Meteorological Applications* (Royal Met.  
891 Society).[doi:10.1017/S1350482703001130](https://doi.org/10.1017/S1350482703001130).
- 892 3. Antón, M., Cachorro, V. E., Vilaplana, J. M., Toledano, C., Krotkov, N. A., Arola, A., Serrano  
893 &Morena, B.,2010. Comparison of UV irradiances from Aura/Ozone Monitoring Instrument  
894 (OMI) with Brewer measurements at El 349 Arenosillo (Spain)–Part 1: Analysis of parameter  
895 influence. *Atmospheric Chemistry and Physics*, 10(13), 5979-350 5989.
- 896 4. Arola A, Kalliskota S, den Outer PN, Edvardsen K, Hansen G, Koskela T, Martin TJ,  
897 Matthijsen J, Meerkoetter R, Peeters P, Seckmeyer G, Simon PC, Slaper H, Taalas P, and  
898 Verdebout J., 2002. Assessment of four methods to estimate surface UV radiation using satellite  
899 data, by comparison with ground measurements from four stations in Europe. *Journal of*  
900 *Geophysical Research*107: 4310.
- 901 5. Arola, A., Kazadzis, S., Lindfors, A., Krotkov, N., Kujanpa, J., Tamminen, J., Bais, A., di  
902 Sarra, A., Villaplana, J. M., Brogniez, C., Siani, A.M., Janouch, M., Weihs, P., Webb, A.,  
903 Koskela, T., Kouremeti, N., Meloni, D., Buchard, V., Auriol, F., Ialongo, I., Staneck, M., Simic,  
904 S., Smedley, A., and Kinne, S., 2009. A new approach to correct for absorbing aerosols in OMI  
905 UV. *Geophysical Research Letters*, 36, L22805.
- 906 6. Bais, A. F., Gardiner, B. G., Slaper, H., Blumthaler, M., Bernhard, G., McKenzie, R., Webb, A.  
907 R., Seckmeyer, G., Kjeldstad, B., Koskela, T., Kirsch, P. J., Gröbner, J., Kerr, J. B., Kazadzis, S.,  
908 Leszczynski, K., Wardle, D., Josefsson, W., Brogniez, C., Gillotay, D., Reinen, H., Weihs, P.,  
909 Svenoe, T., Eriksen, P., Kuik, F., and Redondas, A., 1996. SUSPEN intercomparison of ultraviolet  
910 spectroradiometers. *Journal of Geophysical Research: Atmospheres*, 106, 12509-12525.
- 911 7. Bais, A. F., Zerefos, C. S., and McElroy, C. T., 1996. Solar UVB measurements with the  
912 double- and single-monochromator Brewer ozone spectrophotometers. *Geophysical Research*  
913 *Letters*, 23, 833-836.
- 914 8. Bais, A. F., Zerefos, C. S., Ziomas, I. C., Zoumakis, N., Mantis, H. T., Hofmann, D. J., and  
915 Fiocco, G., 1985. Decreases in the Ozone and the SO<sub>2</sub> Columns Following the Appearance of the  
916 El Chichon Aerosol Cloud at Midlatitude. *Atmospheric Ozone*, Zerefos, C. S. and Ghazi, A.  
917 (Eds.), Springer Netherlands.
- 918 9. Bais, A.F., Drosoglou, T., Meleti, C., Kouremeti, N., 2013. Changes in total solar irradiance  
919 measured at Thessaloniki, Greece since 1993 associated with changes in  
920 aerosols. *AdvMeteorolClimatolAtmos Phys*.
- 921 10. Balis, D., Giannakaki, E., Müller, D., Amiridis, V., Kelektoglou, K., Rapsomanikis, S., and  
922 Bais, A., 2010. Estimation of the microphysical aerosol properties over Thessaloniki, Greece,  
923 during the SCOUT-O3 campaign with the synergy of Raman lidar and Sun photometer data.  
924 *Journal of Geophysical Research: Atmospheres*, 115.<http://dx.doi.org/10.1029/2009JD013088>.



- 925 11. Beale, M. H., Hagan, M. T., & Demuth, H. B., 2012. Neural network toolbox™ user's guide. In  
926 R2012a, TheMathWorks, Inc., 3 Apple Hill Drive Natick, MA 01760-2098. www. mathworks.  
927 com.
- 928 12. Bernhard, G., Arola, A., Dahlback, A., Fioletov, V., Heikkilä, A., Johnsen, B., Koskela, T.,  
929 Lakkala, K., Svendby, T., and Tamminen, J., 2015. Comparison of OMI UV observations with  
930 ground-based measurements at high northern latitudes. *Atmos. Chem. Phys.*, 15, 7391-7412.
- 931 13. Bhartia, P.K., Heath, D. F., and Fleig, A. F., 1985. Observation of anomalously small ozone  
932 densities in south polar stratosphere during October 1983 and 1984. Symposium on Dynamics and  
933 Remote Sensing of the Middle Atmosphere, 5th Scientific Assembly.
- 934 14. Bouillon R., Eisman J., Garabedian M., et al., 2006. Action Spectrum for the Production of  
935 Previtamin D3 in Human Skin. CIE Report No 174, Vienna.
- 936 15. Cachorro, V. E., Toledano, C., Antón, M., Berjón, A., de Frutos, A., Vilaplana, J. M., Arola,  
937 A., and Krotkov, N. A., 2010. Comparison of UV irradiances from Aura/Ozone Monitoring  
938 Instrument (OMI) with Brewer measurements at El Arenosillo (Spain) – Part 2: Analysis of site  
939 aerosol influence. *Atmos. Chem. Phys.*, 10, 11867–11880.
- 940 16. Cadet, J.M., Bencherif, H., Portafaix, T., Lamy, K., Nocingwane, K., Coetzee, G. JR., and  
941 Wright, C.Y., 2017. Comparison of ground-based and satellite-derived solar UV index levels at  
942 six south African sites. *Int. J. Environ. Res. Public Health*, E1384.
- 943 17. Chubarova Ne, Yurova Au, Krotkov N, Herman J, Bhartia PK., 2002. Comparisons between  
944 ground measurements of broadband ultraviolet irradiance (300 to 380 nm) and total ozone  
945 mapping spectrometer ultraviolet estimates at Moscow from 1979 to 2000. *Opt. Eng.*  
946 0001;41(12):3070-3081. doi:10.1117/1.1516819.
- 947 18. de Laat, A. T. J., R. J. van der A, M. A. F. Allaart, et al., 2010. Extreme sunbathing: Three  
948 weeks of small total O<sub>3</sub> columns and high UV radiation over the southern tip of South America  
949 during the 2009 Antarctic O<sub>3</sub> hole season. *Geophys. Res. Lett.*, 37,  
950 L14805. doi:10.1029/2010GL043699.
- 951 19. Eide M.J., and Weinstock M.A., 2005. Association of UV Index, Latitude, and Melanoma  
952 Incidence in Nonwhite Populations—US Surveillance, Epidemiology, and End Results (SEER)  
953 Program, 1992 to 2001, *Arch Dermatol.*, 141(4), pp 477–481. doi:10.1001/archderm.141.4.477.
- 954 20. Emde C., Buras-Schnell R., Kylling A., Mayer B., Gasteiger J., Hamann U., Kylling J., Richter  
955 B., Pause C., Dowling T. and Bugliaro L., 2015. The libRadtran software package for radiative  
956 transfer calculations (Version 2.0). *Geoscientific Model Development Discussions*, VOL. 8. doi:  
957 10.5194 /gmdd-8-10237-2015.
- 958 21. Farman, J. C., Gardiner, B. G., and Shanklin, J. D., 1985. Large losses of total ozone in  
959 Antarctica reveal seasonal ClO<sub>x</sub>/NO<sub>x</sub> interaction. *Nature*, 315, 207-210.
- 960 22. Fioletov V. E., McArthur L. J. B., Mathews T. W. and Marrett L., 2009. On the relationship  
961 between erythemal and vitamin D action spectrum weighted ultraviolet radiation. *Journal of*  
962 *Photochemistry and Photobiology B: Biology*, 95, 9-16.
- 963 23. Fioletov, V., Kerr, J., and Fergusson, A., 2010. The UV Index: Definition, Distribution and  
964 Factors Affecting It. *Can J Public Health*, 101 (4).



- 965 24. Fountoulakis I., Bais A. F., Fragkos K., et al., 2016(a). Short- and long-term variability of  
966 spectral solar UV irradiance at Thessaloniki, Greece: effects of changes in aerosols, total ozone  
967 and clouds. *Atmos. Chem. Phys.*, 16, 2493-2505.
- 968 25. Fountoulakis I., Redondas A., Bais A. F., et al., 2016(b). Dead time effect on the Brewer  
969 measurements: correction and estimated uncertainties. *Atmos. Meas. Tech.*, 9, 1799-1816.
- 970 26. Foxall, R.J., Cawley, G.C., Dorling, S.R. and Mandic, D.P., 2002. Error functions for  
971 prediction of episodes of poor air quality. *Artificial Neural Networks-ICANN 2002* (pp. 1031-  
972 1036). Springer Berlin, Heidelberg.
- 973 27. Fragkos K., Bais A.F., Meleti C., Fountoulakis I., Tourpali K., Balis D.S., and Zerefos C.S.,  
974 2014. Variability of a thirty-year record of total ozone derived from a Brewer spectrophotometer  
975 at Thessaloniki and the SBUV version 8.6. E-Proceedings of the XII EMTE National-International  
976 Conference of Meteorology-Climatology and Atmospheric Physics, Vol 1.
- 977 28. Fragkos, K., A.F. Bais, C. Meleti, I. Fountoulakis, K. Tourpali, D.S. Balis, C.S. Zerefos, 2014.  
978 Variability of a thirty-year record of total ozone derived from a Brewer spectrophotometer at  
979 Thessaloniki and the SBUV version 8.6. E-Proceedings of the XII EMTE National-International  
980 Conference of Meteorology-Climatology and Atmospheric Physics, 1.
- 981 29. Fragkos, K., Bais, A. F., Fountoulakis, I., Balis, D., Tourpali, K., Meleti, C., and Zanis, P.,  
982 2016. Extreme total column ozone events and effects on UV solar radiation at Thessaloniki,  
983 Greece. *Theor. Appl. Climatol.*, 505-517. doi: 10.1007/s00704-015-1562-3.
- 984 30. Gao, W., D. Schmoldt, and J. R. Slusser., 2009. *UV Radiation in Global Climate Change: Measurements, Modeling and Effects on Ecosystems*. Springer-Verlag Berlin Heidelberg and  
985 Tsinghua University Press, Beijing, China.
- 987 31. Garane K., Bais A. F., Kazadzis S., et al, 2006. Monitoring of UV spectral irradiance at  
988 Thessaloniki (1990-2005): data re-evaluation and quality control. *Ann. Geophys.*, 24, 3215-3228.
- 989 32. Ghil M, Allen MR, Dettinger MD et al., 2002. Advanced spectral methods for climatic time  
990 series. *Rev Geophys* 40(1:3):1-41.
- 991 33. Gies, P., Roy, C., Javorniczky, J., Henderson, S., Lemus-Deschamps, L., Driscoll, C., 2004.  
992 Global Solar UV Index: Australian Measurements, Forecasts and Comparison with the UK.  
993 *Photochemistry and Photobiology*, 79(1).
- 994 34. Gonçalves, F., Guilherme, F., de Souza, S., Luiz, O, Festa-Neto, C., Sanches, J., Chammas, R.,  
995 Gattas, G., and Eluf-Neto, J., 2011. European ancestry and polymorphisms in DNA repair genes  
996 modify the risk of melanoma: A case control study in a high UV index region in Brazil. *Journal of*  
997 *Dermatological Science*, 64 (1). doi:10.1016/j.jdermsci.2011.06.003.
- 998 35. Gröbner, J., Blumthaler, M., Kazadzis, S., Bais, A., Webb, A., Schreder, J., Seckmeyer, G.,  
999 Rembges, D., 2006. Quality Assurance of spectral solar UV measurements: Results from 26 UV  
1000 monitoring sites in Europe, 2002 to 2004. *Metrologia* 43, S66–S71.
- 1001 36. Herman, J. R., and E. A. Celarier, 1997. Earth surface reflectivity climatology at 340–380 nm  
1002 from TOMS data. *J. Geophys. Res.*, 102(D23), 28003–28011. doi:10.1029/97JD02074.
- 1003 37. Holben, B.N., Eck, T.F., Slutsker, I., Tanré, D., Buis, J.P., Setzer, A., Vermote, E., Reagan,  
1004 J.A., Kaufman, Y.J., Nakajima, T., Lavenu, F., Jankowiak, I., and Smirnov, A.A., 1998.  
1005 AERONET—A Federated Instrument Network and Data Archive for Aerosol Characterization.  
1006 *Remote Sensing of Environment*, 66 (1), pp 1-16. doi:10.1016/S0034-4257(98)00031-5.

- 1007 38. Hornik, K., Stinchcombe M., White, H., 1989. Multilayer Feedforward Networks are Universal  
1008 Approximators. *Neural Networks* 2, 359-366. doi:10.1016/0893-6080(89)90020-8.
- 1009 39. Hülsen, G., Gröbner, J., Bais, A., Blumthaler, M., Disterhoft, P., Johnsen, B., Lantz, K. O.,  
1010 Meleti, C., Schreder, J., Vilaplana Guerrero, J. M., and Ylianttila, L., 2008. Intercomparison of  
1011 erythemal broadband radiometers calibrated by seven UV calibration facilities in Europe and the  
1012 USA. *Atmos. Chem. Phys.*, 8, 4865-4875, <https://doi.org/10.5194/acp-8-4865-2008>.
- 1013 40. Ialongo, I., Casale, G. R., and Siani, A. M., 2008. Comparison of total ozone and erythemal UV  
1014 data from OMI with ground-based measurements at Rome station. *Atmos. Chem. Phys.*, 8, 3283–  
1015 3289.
- 1016 41. IPCC 2014: Synthesis Report. Contribution of Working Groups I, II and III to the Fifth  
1017 Assessment Report of the Intergovernmental Panel on Climate Change [Core Writing Team, R.K.  
1018 Pachauri and L.A. Meyer (eds.)]. IPCC, Geneva, Switzerland, 151 pp.
- 1019 42. Karppinen, T., Redondas, A., García, R. D., Lakkala, K., McElroy, C. T., and Kyrö, E., 2014.  
1020 Compensating for the Effects of Stray Light in Single-Monochromator Brewer Spectrophotometer  
1021 Ozone Retrieval. *Atmosphere-Ocean*, pp. 1–8. doi:10.1080/07055900.2013.871499.
- 1022 43. Kazadzis, S., Bais, A., Amiridis, V., Balis, D., Meleti, C., Kouremeti, N., Zerefos, C. S.,  
1023 Rapsomanikis, S., Petrakakis, M., Kelesis, A., Tzoumaka, P., and Kelektoglou, K., 2007. Nine  
1024 years of UV aerosol optical depth measurements at Thessaloniki, Greece. *Atmos. Chem. Phys.*, 7,  
1025 2091-2101. <https://doi.org/10.5194/acp-7-2091-2007>.
- 1026 44. Kazadzis, S., Bais, A., Arola, A., Krotkov, N., Kouremeti, N., and Meleti, C., 2009b. Ozone  
1027 Monitoring Instrument spectral UV irradiance products: comparison with ground based  
1028 measurements at an urban environment. *Atm. Chemistry and Physics.*, 9, 585 - 594.
- 1029 45. Kazadzis, S., Bais, A., Balis, D., Kouremeti, N., Zempila, M., Arola, A., Giannakaki, E.,  
1030 Amiridis, V., and Kazantzidis, A., 2009a. Spatial and temporal UV irradiance and aerosol  
1031 variability within the area of an OMI satellite pixel. *Atmos. Chem. Phys.*, 9, 4593-4601.  
1032 <https://doi.org/10.5194/acp-9-4593-2009>.
- 1033 46. Kazantzidis, A., Bais, A. F., Topaloglou, C., Garane, K., Zempila, M. M., Meleti, C., and  
1034 Zerefos, C., 2006. Quality assurance of the Greek UV Network: preliminary results from the pilot  
1035 phase operation. *Proc. SPIE 6362, Remote Sensing of Clouds and the Atmosphere XI*, 636229.
- 1036 47. Kolehmainen, M., Martikainen, H., Ruuskanen, J., 2001. Neural networks and periodic  
1037 components used in air quality forecasting. *Atmos. Env.*, 35(5): 815-825. doi:10.1016/S1352-  
1038 2310(00)00385-X.
- 1039 48. Koukouli, M.E., Balis, D.S., Amiridis, V., Kazadzis, S., Bais, A., Nickovic, S., and Torres, O.,  
1040 2006. Aerosol variability over Thessaloniki using ground based remote sensing observations and  
1041 the TOMS aerosol index. *Atmospheric Environment*.
- 1042 49. Krotkov, N. A., J. Herman, P. K. Bhartia, et al., 2002. OMI Surface UV Irradiance Algorithm,  
1043 Algorithm Theoretical Baseline Document: Clouds, Aerosols, and Surface UV Irradiance. P.  
1044 Stammes (ed.), vol. III, ATBD-OMI-03, version 2.0. [http://eosps0.gsfc.nasa.gov/sites/default/files/  
1045 atbd/ATBD-OMI-03.pdf](http://eosps0.gsfc.nasa.gov/sites/default/files/atbd/ATBD-OMI-03.pdf) (2 May 2016).
- 1046 50. Lantz O.K. and Disterhoft P., 1998. Methodology for deriving Clear-sky erythemal calibration  
1047 factors for UV broadband radiometers of the U.S. Central UV calibration facility. *Journal of  
1048 Atmospheric and Oceanic Technology*, Vol. 16 (pp 1736-1752).

- 1049 51. Levelt, P.F., van den Oord, G.H.J., Dobber, M.R., Mälkki, A., Visser, H., de Vries, J.,  
1050 Stammes, P., Lundell, J., Saari, H., 2006. The ozone monitoring instrument. *IEEE Trans. Geo.*  
1051 *Rem. Sens.* 44 (5):1093–1101. <http://dx.doi.org/10.1109/TGRS.2006.872333>.
- 1052 52. Lucas R., McMichael T., Smith W. and Armstrong, 2006. Solar Ultraviolet Radiation: Global  
1053 burden of disease from solar ultraviolet radiation. World Health Organization, Public Health and  
1054 the Environment.
- 1055 53. Lucas, R., Repacholi, M., and McMichael, A., 2006. Is the current public health message on  
1056 UV exposure correct?. *Bull World Health Organ*, 84 (6), Geneva Jun. 2006.doi:10.1590/S0042-  
1057 96862006000600018.
- 1058 54. Mateos, D., Bilbao, J., Kudish, A. I., Parisi, A. V., Carbajal, G., di Sarra, A., Román, R., de  
1059 Miguel, A., 2013. Validation of OMI satellite erythemal daily dose retrievals using ground-based  
1060 measurements from fourteen stations. *Remote Sensing of Environment*, 128, 1-10.
- 1061 55. McKenzie R.L. and Liley J.B., 2010. UV Radiation in Global Climate Change: Measurements,  
1062 Modeling and Effects on Ecosystems. Chapter 2: Balancing the risks and benefits of Ultraviolet  
1063 Radiation. Springer-Verlag Berlin Heidelberg and Tsinghua University Press, Beijing, China.
- 1064 56. McKenzie, R. L., Seckmeyer, G., Bais, A. F., Kerr, J. B., Madronich, S., 2001. Satellite  
1065 retrievals of erythemal UV dose compared with ground-based measurements at northern and  
1066 southern midlatitudes. *Journal of Geophysical Research: Atmospheres*, 106 (D20). doi:  
1067 10.1029/2001JD000545.
- 1068 57. McKinlay A. F. and Diffey B. L., 1987. A reference action spectrum for ultraviolet induced  
1069 erythema in human skin. *CIE J*, 6, 17-22.
- 1070 58. Meleti, C., Fragkos, K., Bais, A. F., Tourpali, K., Balis, D., and Zerefos, C. S., 2012. Thirty  
1071 years of total ozone measurements at Thessaloniki with a MKII Brewer spectrophotometer.  
1072 Quadrennial Ozone Symposium 2012, Toronto.
- 1073 59. Muyimbwa, D., Dahlback, A., Stamnes, J., Hamre, B., Frette, Ø. Ssenyonga, T., and Chen, Y-  
1074 C, 2015. Validation of OMI UV measurements against ground-based measurements at a stations  
1075 in Kampala, Uganda. *EGU General Assembly 2015*, Vienna, Austria, id: 2632.
- 1076 60. Rumelhart, D.E., Hinton, G.E., Williams, R. J., 1986. Learning representations by  
1077 backpropagating errors. *Nature* 323, 533–536.
- 1078 61. Schmalwieser, A. W., Schauburger, G., Janouch, M., Nunez, M., Koskela, T., Berger, D.,  
1079 Karamanian, G., Prosek, P., and Laska, K., 2002. Global validation of a forecast model for  
1080 irradiance of solar, erythemally effective ultraviolet radiation. *SPIE, Optical Engineering*, 41 (12).
- 1081 62. Slaper H., Reinen H. A. J. M., Blumthaler M., et al., 1995. Comparing ground-level spectrally  
1082 resolved solar UV measurements using various instruments: A technique resolving effects of  
1083 wavelength shift and slit width. *Geophysical Research Letters*, 22, 2721-2724.
- 1084 63. Stammes, P. OMI Algorithm Theoretical Basis Document Volume III, August 2002.  
1085 [https://projects.knmi.nl/omi/documents/data/OMI\\_ATBD\\_Volume\\_3\\_V2.pdf](https://projects.knmi.nl/omi/documents/data/OMI_ATBD_Volume_3_V2.pdf) (12 September  
1086 2017).
- 1087 64. Tanskanen A, Krotkov NA, Herman JR, Arola A., 2006. Surface ultraviolet irradiance from  
1088 OMI. *IEEE Transactions on Geoscience and Remote Sensing* 44(5): 1267–1271.
- 1089 65. Tanskanen, A, Lindfors, A., Määttä, A., Krotkov, N., Herman, J., Kaurola, J., Koskela, T.,  
1090 Lakkala, K., Fioletov, V., Bernhard, G., McKenzie, R., Kondo, Yutaka., O'Neill, M., Slaper, H.,

- 1091 den Outer, P., Bais, A., Tamminen, J., 2007. Validation of daily erythemal doses from Ozone  
1092 Monitoring Instrument with ground-based UV measurement data. *Journal of Geophysical*  
1093 *Research: Atmospheres*, 112 (D24), doi:10.1029/2007JD008830.
- 1094 66. Tanskanen, A., A. Arola, J. Kujanpää, 2003. Use of the moving time-window technique to  
1095 determine surface albedo from the TOMS reflectivity data. *Proc. SPIE Vol. 4896*, p. 239--250.
- 1096 67. Tanskanen, A., A. Lindfors, A. Maatta ,et al., 2007. Validation of daily erythemal doses from  
1097 Ozone Monitoring Instrument with ground-based UV measurement data. *J. Geophys. Res.*, 112,  
1098 D24S44.doi:10.1029/2007JD008830.
- 1099 68. Taylor, K.E., 2001. Summarizing multiple aspects of model performance in a single diagram.  
1100 *Journal of Geophysical Research*, 106 (D7), pp. 7183-7192.
- 1101 69. Taylor, M., Kazadzis, S., Tsekeri, A., et al., 2014. Satellite retrieval of aerosol microphysical  
1102 and optical parameters using neural networks: a new methodology applied to the Sahara desert  
1103 dust peak. *Atmos. Meas. Tech.* 7, 3151-3175. doi:10.5194/amt-7-3151-2014.
- 1104 70. Tevini M., 1993. *UV-B Radiation and Ozone Depletion: Effects on Humans, Animals, Plants,*  
1105 *Microorganism, and Materials.* Lewis Publishers, Inc.: Boca Raton.
- 1106 71. Torres, O.,Tanskanen, A., Veihelmann, B., Ahn, C., Braak, R., Bhartia, P. K., Veeffkind, P.,  
1107 Levelt, P., 2007. Aerosols and surface UV products from Ozone Monitoring Instrument  
1108 observations: An overview. *Journal of Geophysical Research: Atmospheres*, 112, D24.doi:  
1109 10.1029/2007JD008809.
- 1110 72. van Geffen, R. van der A, M. van Weele, et al., 2005. Surface UV radiation monitoring based  
1111 on GOME and SCIAMACHY. *Proceedings of the ENVISAT & ERS Symposium*, 6-10  
1112 September 2004, Salzburg, Austria, ESA publication SP-572.
- 1113 73. Vanicek, K., Frei, T., Litynska, Z., and Schmalwieser, A., 1999. *UV Index for the public.*  
1114 *COST-713 Action*, Brussels.
- 1115 74. Vasaras A., Bais A.F., Feister U., and Zerefos C.S., 2001. Comparison of two methods for  
1116 cloud flagging of spectral UV measurements. *Atmospheric Research*, 57, 31–42.
- 1117 75. Webb, A. R., Groebner J., and Blumthaler M., 2006. *A Practical Guide to Operating Broadband*  
1118 *Instruments Measuring Erythemally Weighted Irradiation.* Publication of COST 726 and WMO.
- 1119 76. Weihs, P., Blumthaler, M., Rieder, H. E., Kreuter, A., Simic, S., Laube, W., Schmalwieser, A.  
1120 W., Wagner, J. E., and Tanskanen, A., 2008. Measurements of UV irradiance within the area of  
1121 one satellite pixel. *Atmos. Chem. Phys.*, 8, 5615-5626. <https://doi.org/10.5194/acp-8-5615-2008>.
- 1122 77. WMO, 2007. *Scientific assessment of ozone depletion 2006.* WMO Report No. 50, World  
1123 *Meteorological Organization*, Geneva, Switzerland.
- 1124 78. World Health Organization, International Agency for Research on Cancer, 2008. *Vitamin D*  
1125 *and cancer.* IARC Working Group Reports, WHO Press, 5, 148.
- 1126 79. World Health Organization, World Meteorological Organization, United Nations Environment  
1127 Programme,International Commission on Non-Ionizing Radiation Protection,2002. *Global solar*  
1128 *UV index: a practical guide.* Geneva, Switzerland:  
1129 *WHO.*[http://www.unep.org/pdf/Solar\\_Index\\_Guide.pdf](http://www.unep.org/pdf/Solar_Index_Guide.pdf).
- 1130 80. Zempila M. M., Giannaros T. M., Bais A., et al., 2016(b). Evaluation of WRF shortwave  
1131 radiation parameterizations in predicting Global Horizontal Irradiance in Greece. *Renewable*  
1132 *Energy*, Vol. 86 (pp 831-840). doi:10.1016/j.renene.2015.08.057.

- 1133 81. Zempila M. M., Koukouli M. E., Bais, A., et al., 2016(a). OMI/Aura UV product validation  
1134 using NILU-UV ground-based measurements in Thessaloniki, Greece. *Atmospheric Environment*,  
1135 Vol. 140 (pp 283-297). doi:10.1016/j.atmosenv.2016.06.009.
- 1136 82. Zempila M.M., M. Taylor, M.E. Koukouli, C. Lerot, K. Fragkos, I. Fountoulakis, A. Bais, D.  
1137 Balis, M. van Roozendaal, 2017a. NILU-UV multi-filter radiometer total ozone columns:  
1138 Comparison with satellite observations over Thessaloniki, Greece. *Science of The Total*  
1139 *Environment*, Volumes 590–591, 15 July 2017, Pages 92-106, ISSN 0048-9697.  
1140 <http://doi.org/10.1016/j.scitotenv.2017.02.174>.
- 1141 83. Zempila M.M., Taylor M., Bais A., and Kazadzis S, 2016(c). Modelling the relationship  
1142 between photosynthetically active radiation and global horizontal irradiance using singular  
1143 spectrum analysis. *Journal of Quantitative Spectroscopy & Radiative Transfer*, 182, 240-263.
- 1144 84. Zempila, M.-M., van Geffen, J. H. G. M., Taylor, M., Fountoulakis, I., Koukouli, M.-E., van  
1145 Weele, M., van der A, R. J., Bais, A., Meleti, C., and Balis, D., 2017b. TEMIS UV product  
1146 validation using NILU-UV ground-based measurements in Thessaloniki, Greece. *Atmos. Chem.*  
1147 *Phys.*, 17, 7157-7174. <https://doi.org/10.5194/acp-17-7157-2017>, 2017.
- 1148 85. Zerefos, C. S., 2002. Long-term ozone and UV variations at Thessaloniki, Greece. *Physics and*  
1149 *Chemistry of the Earth, Parts A/B/C*, 27, 455-460.
- 1150 86. Zerefos, C., 1984. Evidence of the El Chichón stratospheric volcanic cloud in Northern  
1151 Greece. *Geofísica Internacional*, 23.
- 1152 87. Zerefos, C., and Bais, A., 1997. *Solar Ultraviolet Radiation: Modeling, Measurements and*  
1153 *Effects*. Springer-Verlag Berlin Heidelberg.

## Highlights

- Validation of OMI CIE dose rates against several types of ground-based measurements
- Different ground instruments, averaging practices, limitations, cloud conditions
- The OMI CIE dose rate SZA, Ozone, AOD, and cloudiness dependences were examined
- The OMI UVIs were classified and validated for health related public alerts